The morpho-tectonic setting of the South East margin of Iberia and the Adjacent Oceanic Algero-Balearic Basin

Acosta* [a] J., Fontán[a] A., Muñoz[b] A., Muñoz-Martín[c] A, Rivera[a], J., and Uchupi[d] E.

a) Spanish Oceanographic Institute. Servicios Centrales. C/ C. de Maria 8. 28002 Madrid (Spain)

b) Tragsa-SGP, C/Julián Camarillo 6B, 28037 Madrid. (Spain).

c) Universidad Complutense. Fad. CC. Geologicas. C/ J.A. Novais, 2. 28040 Madrid (Spain).

d) Woods Hole Oceanographic Institution. Woods Hole, MA 02543 (USA)

*** Corresponding author:** E-mail: juan.acosta@md.ieo.es. Phone: +34 91 5107500. Fax: +34 91 5974770

Abstract

Multi-beam bathymetry and high-resolution low-penetration seismic reflection profiles of the offshore extensions of the Bétic Internal Zone off Sierra de Cartagena-La Unión margin along its south side and the Mar Menor margin along its east side, the Mazarrón Escarpment forming its southern boundary and the adjacent oceanic Algero-Balearic basin have provided images of the neo-tectonic structures of the region equal to those provided by subaerial photography. For the first time we mapped with unprecedented detail the Mazarrón Escarpment and the Southeast margin of Iberia.

The first-order structures of the region are due to the consequence of the collision of the African and Eurasian plates during the Alpine orogeny in late Oligocene-Middle Miocene, the westward migration of the Alborán plate in the Middle Miocene and the desiccation of the Mediterranean in the Messinian (Late Miocene) that led to the deposition of evaporites in the Algero-Balearic basin and erosion of the Mazarrón Escarpment, the Sierra de Cartagena-La Unión shelf, the Mar Menor margin and the adjacent coast. Our data images second order tectonic features (neo-tectonic features) superimposed on the larger structures. These include the deformation of the strata in the Algero-Balearic basin by the gliding of the Plio-

Quaternary sediments on Messinian halite on the margins of the basin and sediment loading in its center, the Late Miocene-Quaternary deformation of the area north of the Mazarrón Escarpment resulting from the continuous oblique convergence of the African and Eurasian plates in a NNW-SSE direction, the Miocene to Pleistocene volcanic edifices and pinnacles (dikes), the pockmarks formed by the extrusion of gas/water via faults and the massive gravitational failure of the Mazarrón Escarpment triggered by this plate convergence. The data also show in detail features formed on the Mazarrón Escarpment during the Messinian, Pliocene and Pleistocene regressions and those on the shelf formed during the Pleistocene glacially induced regressions/transgression and sediment drifts generated by modern currents.

Keywords: Mazarrón Escarpment; Algero-Balearic Abyssal Plain; Messinian Diapirs; African-Eurasian Plates; Faults; Pockmarks; Seismicity; Bétic Cordillera.

1. Introduction

The Algero-Balearic Basin and the adjacent Spanish margin consist of two distinct tectonic realms. The Iberian continental margin is the creation of the convergence of the African and Eurasian plates during the Alpine orogeny in Late Oligocene-Middle Miocene. The Algero-Balearic Basin is an oceanic basin formed by the western migration of the Alborán plate in Middle Miocene. The east-west trending Mazarrón Escarpment, a right-lateral transform, separates the two realms.

The objectives of the present investigation were to determine the morphology of the offshore extension of the terminal splay of the Eastern Bétic Shear Zone in the Internal Zone, to define its shallow structure, to integrate these data to determine the geodynamic setting of the offshore extension of the Bétic Internal Zone and finally to compare the onshore and offshore settings of the zone (Fig.1). The Internal Zone,

extending from east of the Strait of Gibraltar to the Mediterranean, is comprised of three nappe complexes of variable metamorphic grade and Triassic to lower Neogene (Azañón et al, 2002). The Neogene deformation was accompanied by subsidence of Neogene basins and uplift of the pre-Neogene basement creating a discontinuous chain of sierras separated by Miocene-Quaternary basins (Huibregtse et al. 1998; Woodside and Maldonado, 1992; Silva et al., 2003, 2004).

We extended our study southward as to include the 2800 m deep, 100-120 km wide and 400 km long Algero-Balearic basin. Its oceanic crust, inferred by Panza et al. (2007) to be of Middle Miocene age, is mantled by approximately 1.8 km of Miocene sediments that include less than 1 km of Messinian evaporites (Gallart et al., 1995; Sábat et al., 1995; Mauffret et al., 2004). Deposition of the Messinian evaporites is a result of the closure of the portal between the Atlantic and the Mediterranean by Late Miocene compressional tectonics (Duggen et al., 2004).

2. Area of Investigation and methods used

The offshore extension of the Bétic Internal Zone and adjacent Algero-Balearic Basin investigated during the present study are depicted in Figs. 1 and 2. It has maximum extensions of 334 (east-west) x 130 (north-south) km. The area was surveyed with two Simrad multi-beam systems. An EM-3000 D system (300 kHz) was used in depths of less than 150 m aboard R/V Emma Bardán in cruises during 2001 and 2003 and a Simrad EM-300 (30 kHz) for greater depths aboard the R/V Vizconde de Eza during cruises in 2003, 2004, 2007, 2010 and 2011 (this last year only working with Topas PS18). Information on the shallow structure of the area was obtained with a hull mounted Topas PS 18 High-resolution parametric profiler system, with integrated transmitter and receivers. Navigation was via a differential GPS Simrad GN33 using satellite corrections from a Fugro system integrated in a MDM 400

software package with an inertial integrated aided Seapath 200 System for an accuracy of 0.7 Rms. The multi-beam data sets from Capesme Project (present paper) is gridded at 50x50 meter, Espace Project (present paper) is gridded at 5 x 5 meter. Sbal Deep Project has a 200 x 200 m grid and Balcom Project have a 50 x 50 meter of grid size.

3. Geomorphic Setting

3.1. The Coastal Zone

Three geologic terranes dominate the eastern end of the Bétic Internal Zone. Along the E-W trending coast, at the southern end of the zone, is the 30 km long and 8 km wide Sierra de Cartagena-La Unión (Fig. 1; López-Ruiz et al., 2002; Duggen et al., 2005). It has a relief of 0-400 m and high slopes a result of its proximity to the coast (Conesa and Jiménez-Cárceles, 2007). At its eastern tip is Cabo de Palos where Miocene volcanics rest on Bétic Internal Zone strata (Jiménez-Martínez et al., 2012). The Internal Zone units are locally covered by Miocene-Quaternary sediments and cut by NW-SE-and E-W-trending fault systems formed during the Eocene and Middle Miocene (Robles-Arenas and Candela, 2010). A Middle Miocene reactivation of the fractures led to the formation of a series of horst and graben structures (Manteca and Ovejero, 1992). As a consequence of tectonic activity during the Late Miocene-Pliocene rhyolites-dacites, andesites and alkaline basalts were extruded along these faults (Duggen et al., 2005; Robles-Arenas and Candela, 2010; Jiménez-Martínez et al., 2012). According to Manteca Martínez and Ovejero Zappino (1992), Azañón et al. (2000), Robles-Arenas and Candela (2010) those E-W trending faults and the NW-SE trending transcurrent faults in the coastal area between Mazarrón and Cabo de Palos appear to be related to recent tectonic events involving strike-slip and compression.

North of the Sierra de Cartagena-La Unión is the Neogene Murcia Basin whose top, the Campo de Cartagena, have an area of 1440 km^2 (Jiménez-Martínez et al, 2012). The Campo de Cartagena represents the subaerial westward extension of the Mar Menor Shelf level (Jiménez-Martínez et al, 2012). The sediment cover atop the Bétic System consists of Neogene and Quaternary strata with a maximum thickness of 2000 m. The Neogene sequence is deformed by normal faults and joints some of which affect the Quaternary. Jiménez-Martínez et al, (2012) reported that the Quaternary sediments that cover much of the Campo de Cartagena have been affected locally by recent tectonic activity.

At the eastern end of the Campo de Cartagena is the Mar Menor, a triangular-shape coastal lagoon with dimensions of 13x15x21 km, a mean depth of 2.5m and a maximum depth of 6 m. It is separated from the open sea by a 20 km long and 100-900 m wide barrier island, La Manga (Conesa and Jiménez-Cárceles, 2007). At the southern end of La Manga is Cabo de Palos consisting of 14 small ledges composed of Miocene volcanics (López-Ruiz et al., 2002). Within the lagoon are five islands composed of Miocene volcanics (López-Ruiz et al., 2002).

North of Mar Menor are the NE-trending Torrevieja and Pedraza-Guardamar anticlines and the E-W- trending anticline south of Pinet Lagoon, the Santa Pola Anticline and an anticline north of Santa Pola (Soria et al., 2008). Along the northwest side of the Pedraza structure is the E-W- trending left-lateral Bajo Segura Fault. Cutting across both anticlines are NW-SE San Miguel, Torrevieja and Guardarmar right lateral faults (Alfaro et al., 2002b; Soria et al., 2008). North of the Bajo Segura fault is the Bajo Segura basin flanked on its northwest side by the northeast trending Crevillente anticline and left-lateral Crevillente fault. This fault forms the boundary between the Bétic External zone to the northwest and the Internal Zone to the southeast (Reicheter and Reiss, 2001).

3.2. The Mar Menor and The Sierra de Cartagena-La Unión Continental Shelves

The Mar Menor Shelf, east of Mar Menor, is 32 to 42 km wide and that south of Sierra de Cartagena-La Unión is 10 to 3 km wide (Figs.1 and 2; Table 1). Off La Manga, at depths of 10 to 20 m, are three volcanic islands of the Isla Grosa group. Farther east, at a depth of about 58 m, is the three islands of the SW-NE trending Islas Hormigas group. The shelf's edge east of Mar Menor is about 200 m and that south of Sierra Cartagena ranges from 146 m in the east to 78 m in the west.

On the shelf east of Mar Menor are at least eight relic barrier islands with the easternmost trending north-south and the western ones (bars 7 and 8; Fig. 3 B) trending slightly west of north and parallel the present one, La Manga. Between the relict bars are northeast-southwest trending sediment waves with their steep sides facing southeast. Similar, but having less reliefs also occur in secondary bars between bars 7 and 8 parallel to La Manga (Fig. 3B). These sediment drifts have been reported as far north as the Columbretes Islands at 39˚53'N; 0˚40'E (Fig. 1; Muñoz et al., 2005). We propose that they are being formed by southwest flowing current known as the Liguro-Provençal-Catalán Current or North Current (Font et al., 1995). Some of the sediments transported southward by the North Current may be trapped by the east-west trending Torrevieja half-graben and then transported eastward into the deep-sea (Fig. 4A). Off Cabo de Palos is a chain of rocky ledges, representing dikes, trending northeastward in the direction of Islas Hormigas (Fig. 3B and General Map.tif in the web version). They were probably extruded along a fault trending in that direction. The three islands of the Isla Grosa group and the three islands of the northeast-southwest trending Islas Hormigas group also are of volcanic origin and are correlative with the Miocene volcanic islands in Mar Menor and the seamounts on the slope (inner San Pedro Basin; see below) east of the shelf. The sediment drifts have

preferentially accumulated on the northwest side of the rocky ledges off Cabo Palos. Gaps between them have served as portals for sediment transport to the southeast. Along the southeast of the rocky ledges also are bottom current created scours.

At the east end of the Sierra de Cartagena-La Unión Shelf, is an irregular outlined pavement whose surface is scarred by north and northwest trending lineations which we speculated is a rocky surface, possibly a seaward extension of the Sierra de Cartagena-La Unión (Fig. 3C). Along its western edge is a chain of pimple-like highs of less than 1 m relief of unknown origin and composition. They could represent igneous dikes as Miocene-Pliocene volcanism occurs in the sierra (Robles-Arenas and Candela, 2010). This rocky pavement forms the top of a broad swell whose outer edge is relative smooth to undulating. The seafloor to the southeast of the swell is irregular, displaying a patch of flat-floored irregular outlined lows that may be the result of sediment sheet flow. This topography extends to the shelf edge and terminates westward against a northwest trending scarp that extends across the shelf. This scarp with a relief of 30-40 m may represent a fault scarp. Farther west, the Sierra de Cartagena-La Unión Shelf surface is dominated by northwest-southeast aligned lineations with reliefs of 4 m that extend across much of the shelf (Fig. 3C). They too may represent fault scarps. Superimposed on these larger structures is an extensive field of sediment waves with amplitudes of 25 cm and trending north-northwest. As imaged in Fig. 2A along the edge of the shelf in front of Sierra de Cartagena-La Unión, are promontories that divide the heads of submarine canyons. Both, the heads of the canyons and promontories display features suggestive of mass movements with the canyons serving as pathways down the Mazarrón Escarpment for the displaced sediments. The Sierra de Cartagena-La Unión Shelf off Águilas is 4.7 km wide and shows a 7.5 by 2.8 km sediment wave field from Cabo Cope to Águilas, between 56

and 81 m water depth. The waves have amplitudes of 1 m, their crest are oriented NNW-SSE, and they seems to be bounded by NW-SE faults (Fig. 3D).

3.3. Mar Menor Slope

The morphology of the Mar Menor Slope is shown in the Digital Terrain Model (DTM) in Figs. 2A, and the 3D bathymetry views of Fig. 4A. The upper Mar Menor Slope descending from the Mar Menor Shelf edge at a depth of 200 m bottoms out on a terrace at a depth of 400 m. Its surface has a slope of 0˚40’ and is smooth. The slope segment descending from this terrace displays two surfaces, one from 400 to 525 m that has a slope of 0˚30’ and another from 525 to 625 m with a gradient of about 2˚. Along the northern edge of the shallower surface is a flat-top seamount with a relief above the seafloor of about 200 m and whose top is at a depth of 225 m. Along its north side is a lenticular-shaped depression. Scattered over this surface is a vast network of circular depressions with diameters of several hundred meters and relief from 5 to 60 m below the surrounding sea floor. The slope segment from 525 to 625 m depth also displays circular depressions. On the eastern side of this surface, is a 1.5 x 4.5 km seamount with a sharp crest at a depth of 375 m. Along the west side of this seamount also is a lenticular depression. From 625 to 2700 m the gradient of the Mar Menor Slope increases to 4˚ and its sides are deeply cut by gullies. The seafloor beyond this scarp is relatively smooth and terminates against an N-S trending high whose sides are scalloped and cut by gullies draining east and west. An aerial view of the Mar Menor shelf and slope imaged in Fig.4A displays the smooth topography of the shelf and upper slope with the lower slope divided into three gullied lobes separated by east-west trending narrow troughs.

Along the Northeast-Southwest side of the Mar Menor slope is a flat-floored channel (Torrevieja Half-Graben; Fig. 4A). At its head is a 15 km wide fan that

terminates against the base of the Mar Menor slope and whose surface is disrupted by a chain of depressions oriented East-West. The channel drains into the Algero-Balearic Abyssal Plain via a 2 km wide gap at 0˚ 33'E between Mar Menor Slope and the N-S high. A 12 km wide N-S trending gap east of the N-S trending high also links the channel with the Algero-Balearic Abyssal Plain (Fig. 2A). This path is divided in two by two low relief highs oriented parallel to its axis.

The surface of the Algero-Balearic Abyssal Plain, is disrupted by intrusives rising tens of meters above its surface (See next section) and a few km wide furrows trending N-S and NE-SW. About 15 km northeast of the mouths of the channel, in the abyssal plain, the diapirs form a circular structure with a diameter of 14 km (Fig. 2B).

The scarp, probably a fault scarp, along the NE side of the channel (Figs. 2A and 18) is cut by gullies and divided in two by a 5 km wide gap at 0˚30E. The gap has a V-shaped cross section, steep side slopes is cut by gullies and have a smooth floor. West of this gap, along the crest of the scarp, is Don Juan Seamount described by Maillard and Mauffret (2011). West of the seamount is a platform dipping northward. Cutting across this platform is a northwest trending low relief swell with circular depressions along its crest. The seafloor immediately to the northeast consists of a smooth floored low, bordered on the northeast by an irregular slope facing southwest. Farther northeastward the topographic trend changes from NW to NE. As mapped by Camerlenghi et al. (2009) this terrain, south of Formentera (Fig. 1), consists of concave erosional escarpments, from which a dendritic drainage system originates (Fig. 2A).

3.4. Mazarrón Escarpment

The Mazarrón Escarpment is located south of Sierra de Cartagena-La Union and the Mar Menor slope. It has a total length of 145 km long, 7 to 19 km wide and

has a maximum relief of 2,300 m with a gradient that ranges from 14 to 31 degrees (Fig. 2B). Its crest ranges in depth from 2,400 m at its eastern end to 225 m at the southern edge of the Mar Menor Shelf, 112 to 149 m along the Sierra de Cartagena-La Unión Shelf edge from 0˚45'W to 1˚15' and 676 m at 1˚45'W west of the present survey. From 0˚43'W to 0˚ 33'W the scarp is disrupted by a 25 km wide and about 5 km deep south facing embayment. East of this embayment, at 0˚30'W, the scarp is partially offset in two by a northeast trending ramp that extends halfway down the scarp (Fig. 4A). The floor of the ramp is relatively smooth and its north slope displays a smooth topography to the east and gullied one toward the west (Fig. 4A). The Mazarrón Escarpment displays distinct morphology on either side of the ramp. Extensive slumps front the segment of the Mazarrón Escarpment west of the ramp with many of them covering the lower part of the scarp (Fig. 4B). West of the ramp, the top of the scarp is convex southward, and east of the ramp the scarp is made of two segments separated by a north-south trending east facing slope at about 0˚10'W that we infer is the trace of a fault. West of this fault the Mazarrón Escarpment is displaced to the south and is somewhat convex in outline. East of this fault the Mazarrón Escarpment is more linear, trends east-west and gradually decreasing in relief, ending abruptly along the west side of a north-south trending channel.

The Mazarrón Escarpment west of the ramp, like the Emile Baudot Escarpment east of 2˚ E (Fig. 1), is cut by short canyons (Fig. 2A; Table II). The divides between the canyons are very narrow, in the order of a few km or less and are sharp crested. The canyons heads indenting the outer shelf are convex in shape and are cut by numerous gullies. Side-scan sonar data also indicate that the sharp-crested divides form the apex of chevron-patterned gullies cutting the sides of the canyons (Woodside et al., 2000). Flat-iron morphology also is present on some of the distal ends of the canyon divides east of the ramp (Fig. 4C). On land such morphology is created by

differential erosion of a resistant rock dipping in the same direction, but at a steeper angle than the mountain slope. Their limited distribution offshore suggests that may not have originated in this manner.

The canyons west of the ramp have channel extensions onto the uppermost continental rise (Fig. 2B), but those east of the ramp end abruptly at or near the base of the scarp (Fig. 4C). The canyons east of the ramp also are more subdued and appear to be older than that west of the ramp. They lack slumps at their mouths and the Algero-Balearic Abyssal Plain is separated from the Mazarrón Escarpment by a narrow continental rise or abuts the scarp. The heads of two of the canyons, at 0˚10'W (east of the ramp) and about 0˚35'W (west of the ramp) are unusually wide, probably as a result of mass wasting (Figs 2, and 4A). Most of the canyons, east and west of the ramp, trend N-S and have reliefs of several hundred meters. Three of the canyons (Tiñoso, Cartagena E, and Cartagena W canyons), between 0˚30'W and 0º45'W, west of the ramp, display channel extensions in the upper rise that cut the slumps at the base of the Mazarrón Escarpment (Figs. 2 and 4B). The westernmost one (Cartagena W Canyon) cuts a spur at the base of the scarp in two and another first flows parallel to the scarp and then changes its course abruptly to the southeast on the rise as it cut through the a 45 km long and 15 km wide area of rough topography. This topography is at the mouth of the 47 by 33 km embayment entrenched on the Mazarrón Escarpment from 0˚43'W to 0˚ 33'W (Fig. 4B). The third continental rise channel extension is along the base of the scarp along the contact between the rough topography and the scarp draining eastward of the ramp (Fig. 4B).

Near 0˚15'W this channel turns southward at the east end of the rough topography and drains into a smooth area between the intrusions in the Algero-Balearic Abyssal Plain. This smooth topography, with five intrusions rising above its general level, extends to the eastern end of the Mazarrón Escarpment. An over 50 km

long ridge that meanders along its strike forms its southeast border (Fig. 4A). That few of the intrusions on the rise and abyssal plain occur within this smooth section suggests that deposition exceeds the growth of the intrusions. One of the canyons east of the ramp cuts deeply into the seamount slightly west of 0˚ (Seco de Palos Seamount) with the canyon immediately east of the seamount being oriented obliquely to the Mazarrón Escarpment (Fig. 4). The presence of this volcanic edifice suggests that differences in the morphology of the Mazarrón Escarpment east and west of the ramp at 0˚30'W may be due to the possibility that the scarp east of the ramp in part consists of volcanics. As displayed in the 3D bathymetry in Fig. 4A canyon cutting the Sierra de Cartagena-La Unión Shelf appear to be concentrated into the strata below the Plio-Quaternary surficial sediments covering the shelf.

3.5. Continental Rise and Algero-Balearic Abyssal Plain

The continental rise south of the Mazarrón Escarpment is best developed west of 0˚15'W. It appears to be missing or is very narrow in an embayment of the Mazarrón Escarpment at 1˚W (Fig. 2). From 0˚15'W to about 0˚ 30'W the rise displays noticeable relief, a rough terrain flanked on its west side by a tens of meters high northwest-southeast trending spur oblique to the base of the Mazarrón Escarpment. Located at its tip is Águilas Seamount (Fig 4B). East of 0˚15'W the continental rise is missing or poorly developed and the Algero-Balearic Abyssal Plain extends to or near the base of the Mazarrón Escarpment. An abyssal plain appears to occupy an embayment in the Mazarrón Escarpment at 1˚W. North of 37˚40'N and east of 0˚30'E the Algero-Balearic Abyssal Plain southeast of the Ibiza Channel is bordered on the east by a NW-SE trending less than 100 m high scarp (Fig. 1A). West of 0º50'E the top of the scarp is mantled by a sediment apron extending northward to the base of a rough surfaced several hundred meters high scarp. A 20 km wide gap

cuts the scarp in two at 0º 50'E with the ridge segment southeast of the gap having a sharp crest with its flanks cut by gullies draining north and south. The gap in the ridge appears to have served as a pathway for sediments draining southward from the rise northeast of the ridge. Furrows oriented at right angles to the ridge cut the seafloor northeast of the ridge. Southwest of the ridge (Fig. 1A), the abyssal plain is cut by a 3 to 1.5 km long and several hundred meters wide furrows oriented northeast-southwest. At the northern edge of the abyssal plain also is a circular structure with a diameter of 14 km consisting of short parallel highs separated by about hundreds of meters wide troughs.

Rising from the surface of the Algero-Balearic Abyssal Plain south of the Mazarrón Escarpment in the Mar Menor Margin are N-S, E-W and NE-SW trending highs with reliefs of <40 m and lengths of 2 to 50 km (Fig. 1B). They are in the form of ridges that meander and widen along their lengths, blister-like highs with a tail, an ellipse with a 100 m wide depression in the middle, rods some of which have depressions along their axes, mounds, others resemble fish-hooks or in the form of a "T" shaped low with raised rims. At the western end of the field, slightly east of 1˚W, the north side of one of the structures displays a system of channels that diverge toward the north. South of this high are two 10 km long, parallel ridges that are 5 km apart.

4. Seismic Stratigraphy

Information on the shallow structure of the area was obtained with a hull mounted Topas PS 18 High-resolution parametric profiler system, with integrated transmitter and receivers. The acoustic stratigraphy imaged by these profiles coupled with the multi-beam we use below to reconstruct the geologic fabric of the offshore extension of the terminal splay of the Eastern Bétic Shear Zone in the Internal Zone.

4.1. The Mar Menor and The Sierra de Cartagena-La Unión Continental Shelves

The acoustic stratigraphy of the Mar Menor Shelf is displayed in Figs. 5 and 6, whose locations are shown in Fig. 2A. Line 062 (Fig. 5A) in the Mar Menor Shelf off Torrevieja, images two of the relict barrier islands and a stratified sequence (LS?) between them that we infer are lagoon sediments deposited behind the barrier islands. The barriers consist of some strong reflecting material masking the reflectors beneath them. Line 036 (Fig. 6A) extends across the topographic bank on the outer edge Mar Menor Shelf to the ramp cutting the Mazarrón Escarpment in two at 0˚ 30'W. The high has a flat-top whose depth is 0.2 seconds (150 m) and parts of its south and east sides are exposed. Possibly the strata below this surface (R) may be equivalent to IZ (the Bétic Internal Zone) in the Sierra de Cartagena-La Unión Shelf. Its north side is covered by two sequences separated by an irregular unconformity dipping northward. The lower unit resting unconformably on the north dipping side of the high is acoustically transparent and is about 0.05 seconds thick. The stratified sequence above the transparent unit is 0.05 seconds thick and consists of two sediment units with the upper one being more reflective; both units display southward prograding geometry. The south side of the high, descending to the ramp dividing the Mazarrón Escarpment in two, is onlapped by sediments extending down to the ramp's axis. The sediments on the south slope of the ramp dips northward with a reversal in dip from south to north. Such a reversal may be indicative of a fault. Line 037 (Fig. 6B), east of 036, also extends from the top of the bank, probably cored with IZ strata, to near the top of the Mazarrón Escarpment. Possibly one of the topographic irregularities on the bank may be of fault origin as its southern side. Along this line the bank displays no acoustic penetration and its southern faulted slope is onlapped by two sequences resting

unconformably on one another. The upper unit is deformed at its lower end, an irregularity that may be the result of faulting.

The N-S-trending Line 011 (Fig.5B) in the Sierra de Cartagena-La Unión Shelf displays three terraces (T) at 0.035, 0.040 and 0.045 seconds (or 26, 30 and 34 m; based on a velocity of 1500 m/sec) at the north end of the profile. A gently undulating strong reflecting surface, R, at a depth of 0.10 seconds (75 m; based on a velocity of 1500 m/sec) extends across much of the profile. We infer that R is an erosional surface cut during the Holocene transgression. Projection from coastal exposures suggests that unit IZ on which R was eroded represents the Bétic Internal Zone of the Sierra de Cartagena-La Unión; (see Discussion; Section 6.1). At the outer shelf on profile 011 (Figure 5B) a 4.5 km wide terrace, backed by 50 milliseconds high scarp, has been cut on the R into the Bétic Internal Zone of the Sierra de Cartagena-La Unión strata. These strata are exposed on the Mazarrón Escarpment. The sediment cover on the terrace displays evidence of reworking. Along Line 010 (Figure 5C) the R surface is exposed on the inner shelf. Sediments prograding over the R surface has led to the formation of a wave built terrace (T) at a depth of 0.070 seconds (53 m). Seaward of this terrace the R surface, which dips gently seaward, is covered by sediments about 0.050 seconds thick. The outer edge of this sediment cover is cut by a terrace at a depth of 0.150 seconds (113 m). The terrace is backed by a south facing 30 m high scarp. At the base of this scarp is a few hundred meters wide wave cut terrace on which R is exposed and the strata of the Bétic Internal Zone crop out. These rocks also are exposed on the crest of the Mazarrón Escarpment at a depth of 140 m.

Along Line 009 the Sierra de Cartagena-La Unión Shelf consists of an acoustically transparent unit 0.06 to 0.02 seconds thick capped by R. This unit is divided in two by a reflector at a depth of 0.02-0.03 seconds below the seafloor that onlaps northward (landward) on IZ at a depth of 0.02 seconds. Above Reflector R are

acoustically transparent sediments less than 0.001 seconds thick. The north-south trending Line 001 (at 1˚24'W; west of the present survey) on Fig. 7 indicates that the mid to outer shelf seaward facing scarp is the front of a sediment wedge. The scarp has a relief of 0.17 seconds (128 m) and the sediments behind it are acoustically transparent. Its edge is at a depth of 68 m. The wedge, representing the inner shelf, rests unconformably on a sequence of parallel reflectors dipping southward to a depth of 0.90 seconds (675 m) to the crest of the Mazarrón Escarpment. The top of these reflectors with a southerly gradient of 1˚ forms the outer shelf.

The acoustic stratigraphy of the Sierra de Cartagena-La Unión Shelf is different from that of the Mar Menor Shelf. East of 1˚W the shelf is a seaward dipping platform terminating on a tens of meters high scarp resting on the crest of the Mazarrón Escarpment. Along one seismic profile (Line 011; Fig. 5B) the scarp along the shelf edge has experienced erosion. Along its base is a wave built terrace seaward which is a narrow platform, probably cored with Bétic rocks. Along a profile west of line 011 (line 010; Fig. 5C) the scarp is separated from the Mazarrón Escarpment by a narrow terrace on which the Bétic Internal Zone metamorphic complexes also crop out. On Line 009 (Fig. 5D), farther west at 0.55'W, the scarp along the seaward edge of the inner shelf is on the top of the Mazarrón Escarpment and the Bétic rocks crop out at a depth of 113 on the Mazarrón Escarpment. West of this line the scarp along the shelf's edge displays an undulating aerial view, trends E-W and gradually migrates northward from the Mazarrón Escarpment as the Mazarrón trend changes from E-W to NE-SW. Still farther west the scarp separating the inner and outer shelf is at a considerable distance from the Mazarrón Escarpment (Line 001; Fig.7). The inner shelf and scarp lack stratification and the outer shelf consisting of a sequence of parallel reflectors pinching out on top of the Mazarrón Escarpment at a depth of 675 m at the top of the Mazarrón Escarpment. The top of the Bétic rocks is not imaged along

the length of this profile. Apparently the top of the Bétic rocks is beyond the limit of the penetration of the seismic system used. Comparison of lines 011, 010, 009 and 001 indicates that the top of the Bétic rocks deepens westward with a concurrent thickness of the strata resting on the Bétic.

The relationship between the Mazarrón Escarpment and the scarp separating the inner and outer Sierra de Cartagena-La Unión Shelves is illustrated by the 3D bathymetry in Fig. 4A. East of Cape Tiñoso the shelf is one continuous surface extending to the top of Mazarrón Escarpment and the scarp is along the top of the Mazarrón Escarpment. West of this cape the shelf consists of two surfaces, the inner and outer shelves, and the scarp is at some distance north of the Mazarrón Escarpment. Along line 001 (Fig. 7) the scarp has a relief of 0.125 seconds (93.75 m) and is bordered on the southern side by a gently seaward plain (the outer shelf) that intersecting the Mazarrón Escarpment at a depth of 0.9 seconds (675 m; based on a velocity of 1500 m/sec). The cause or causes of this northward migration of the scarp is to be resolved

4.2. The Torrevieja Half-Graben and the San Pedro Basin (Mar Menor Slope)

The onshore area of the Mar Menor margin represents the terminal splay of the Eastern Bétic Shear Zone (Bousquet, 1979; Alfaro et al., 2002a, 2002b; Silva et al., 2004; García-Mayordomo and Martínez-Díaz, 2006). Deformation on the splay that occurred from Late Miocene to the present, is driven by the NW-SE convergence of the African and Eurasian plates at a rate of 4-5 mm/yr, a convergence accommodated by folding and reverse and right-lateral faulting of the sediment cover onshore (de Mets et al, 1990). Alfaro et al. (2002b) stated that the deformation of the onshore upper Miocene-Quaternary in southeast Spain continues offshore forming an ENE-WSW 20-30 km wide and at least 80 km long anticlinorium, the Tabarca

anticlinorium, extending along the coast from Santa Pola to Torrevieja. Recent faults and folds have uplifted this structure (Alfaro et al., 2012). Maillard and Mauffret (2011) stated that the Tabarca anticlinorium (also known as the Tabarca High) east of 0˚E splits into the Alicante anticlinorium (also known as the Alicante High) and the Elche Ridge (also known as the Elche High) to the north (Fig. 18). Alfaro et al. (2002b) inferred that the deformation offshore is obscured by undisturbed Late Pleistocene-Holocene sediments. However, more recently, Perea et al. (2009, 2010) (Gràcia et al., 2010) and Maillard and Mauffret (2011) reported that the offshore extensions of the onshore folds and faults of the Bajo Segura fault zone are active and reach up to the seafloor.

South of the Tabarca anticlinorium are the E-W trending Torrevieja half-graben and San Pedro Basin (Mauffret et al., 1992; Maillard and Mauffret, 2011; Fig. 8A). From Fig. 6 in Alfaro et al. (2002b) the Torrevieja half-graben appears to be on line with an asymmetrical syncline in their line S8-1-B- 2. It is also on line with subsurface San Javier sub-basin, a graben in the basement in the Murcia basin that is filled with 2000 m of Neogene–Quaternary sediments (Jiménez-Martínez et al., 2012). Northeast of the Torrevieja half-graben (Fig. 8 B-C) is a broadly faulted and folded terrane along the eastern end of the Tabarca anticlinorium. Similar subsurface structures on the shelf were inferred by Alfaro et al. (2002b) to be the product of active reverse faults. At the tops of two of the offshore faults mapped by us are small,"V" shaped depressions that may represent pockmarks created by the expulsion of gas/water. Such circular depressions are quite extensive in the region of the faulted folds (Fig. 18). Associated with two of the pockmarks are mounds with tens of meters of relief (Fig 8B-C). Although we have no samples to verify their origin, we infer that they are mud volcanoes formed from material extruded via the pockmarks. Line 055 (Fig. 9A) cuts across the Don Juan Seamount terminating in the Torrevieja half-

graben. The profile shows that the seamount is fault bound, has a rounded top, that the sediments in the perched basin north of the seamount are stratified and that a high on the north side of the basin is made up of folded sediments. Sediments in the Torrevieja half-graben south of the scarp are stratified with their surface displayed evidence of erosion.

Maillard and Mauffret (2011) inferred that San Pedro Basin (seaward extension of the Murcia basin) is divided in two by Cogedor ridge parallel to the Tabarca anticlinorium. Their Fig. 3 shows the western end of this high at Mar Menor and from there extending eastward to 0˚E. They further postulated that the volcanic edifice, Don Juan Seamount south of Alicante anticlinorium, might be an eastward extension of the Cogedor Ridge. Our interpretation is different. First the Don Juan Seamount is not related to the Cogedor Ridge but forms the northern boundary of the Torrevieja half-graben. Our seismic data suggests that the Cogedor Ridge dividing the San Pedro Basin in two is a volcanic high whose strike is defined by seamounts, volcanic pinnacles and pockmarks in the Mar Menor slope, the volcanic Isla Grosa and Islas Hormigas groups in the Mar Menor shelf, the volcanic islands in Mar Menor and the divide between San Javier and Torre-Pacheco subsurface basins in Campo de Cartagena.

Another high binds San Pedro Basin along its southern margin. This high, whose southern side forms the Mazarrón Escarpment, is in part volcanic as indicated by the presence of Seco de Palos Seamount in Fig.4. This High is the eastern extension of the Internal Zone in the Sierra Cartagena-La Unión.

Sediments on the inner San Pedro Basin (the upper Mar Menor slope) are tectonically undisturbed. A well drilled at a water depth of 144 m at the outer edge of the shelf at 0˚23’54.57’’W; 37˚58’29.58” N consisted of 388 m of Quaternary calcareous muds interbedded with fine sands, 70 m of Quaternary and upper Pliocene

sandy calcareous mud and 120 m of upper Pliocene dolomitic limestones and dolomites (Díaz del Río, 1993). Alfaro et al. (2002b; their Fig. 2) dated the carbonates as Tertiary-Miocene and the terrigenous deposits above it as Plio-Quaternary. They interpreted the upper Tortonian-Messinian sequence as a progressive shallowing upward mega-sequence consisting of pelagic basin facies at the base and shallow marine evaporites and carbonates facies on top.

Lines 035 and 034 (Fig.6 C-D) display the acoustic stratigraphy on the mid San Pedro Basin west and northwest of the bank at the southern end of the Mar Menor upper slope. As imaged by Lines 034 and 035 (Fig. 6) topographic irregularities on upper slope are due solely to bottom currents. The N-S trending Line 034, northwest of the bank, images a complex of sediment drift sequences onlapping the top of the Mazarrón Escarpment. Unit IZ at the bottom of the sequences, may represent the top of the Bétic Interior Zone with the trough cut on the top of the sequences being the creation of bottom current erosion.

The geometry of the drifts is quite complex ranging from a strong reflecting swell, unit's onlapping its southern side, sediments prograding south and north resting on each other with all the units capped by a sequence that extends the length of the profile. Along the NW-SE trending Line 035, that extends from the NW base of the flat-top bank to the eastern edge of the Mar Menor Shelf, the strata on the northern end of the profile displayed a geometry suggestive of bottom current activity with most of the profile consisting of a sequence of parallel reflectors consisting of two units, a well stratified lower and more homogenous upper one. These strata display no evidence of current activity southeast of the Mar Menor Slope. The reflector at the base of the lower unit may be the top of the Bétic Internal Zone.

The acoustic stratigraphy of the outer San Pedro Basin is imaged in the TOPAS seismic reflection profiles in Fig. 10 whose locations are shown in Fig. 2A.

The acoustic stratigraphy displayed by the profiles is one of a prograding folded and faulted wedge onlapping the lower slope. V-shaped notches, some of which are located on the tops of faults, cut the sediments. Cutting through the sediments also are highly reflective pinnacles and a flat-topped seamount whose crest is at a depth of 225 m. A V- shaped convex westward low on the southwest side of the seamount with a maximum depth of 625 m extends from N37˚55'N to about N37˚50' (Figs. 2 and 10A). Sediments on the slope descending westward to a low are faulted.

The folded and faulted sediments in the outer San Pedro Basin are crossed by two north-south trending left lateral faults and is disrupted by four seamounts, circular depressions and intruded by igneous pinnacles of the Cogedor ridge. The faults oriented at right angles to the master fault, the Mazarrón Escarpment, may represent antithetic strike-slip faults. As there is no evidence of bottom current activity in the area, we speculate that the lenticular shaped depressions in the slope are probably due to faulting, not bottom current erosion. We have no information as to the composition or age of the seamounts, which probably represent volcanic edifices. They may be correlative with the volcanic ledges in Cabo de Palos, the ledges and volcanic islands in the Mar Menor Shelf and the volcanic islands in Mar Menor composed of calc-alkaline basalts of Late Miocene age (López-Ruiz et al., 2002).

The pinnacles, probably of volcanic origin, cover an area of 45 x 10 km and are intruded into the Plio-Quaternary sedimentary wedge, demonstrating that they are younger than the seamounts. They are probably Quaternary in age and may be correlative with either the pinnacles in the vicinity of the 1.46± 0.18 my Emile Baudot Seamount south of Mallorca (Acosta et al., 2004) or the pinnacles in the area of the Columbretes Islands at 39˚53'N; 0˚40'E on the outer shelf (Muñoz et al., 2005).

Deformation of the Holocene sediment drift by igneous intrusion, up-doming of the seafloor by an igneous plug, pimples on the seafloor that probably represent the

tops of dikes and their pristine preservation led Muñoz et al. (2005) to infer that the dikes in the Columbretes Islands area at a depth of 80/70 m are Holocene and are younger than 13,000 years when sea level reached an elevation of 60 m below its present level.

At the intersection of some of the faults in the San Pedro Basin with the seafloor, are circular depressions with diameters of tens of meters, but other depressions do not appear to be associated with the faults. We interpret these features as pockmarks formed by the expulsion of gas/water. Their occurrence near the volcanic edifices and their association with faults support the possibility that the pockmarks were formed by the expulsion of gases and associated waters along the faults from a hydrothermal field beneath the surficial sediments. Acosta et al. (2001b) proposed such an origin for the pockmarks in the Ibiza Channel. Possibly, the faults that served as passageways for the gases/fluids reflect deep structures, beyond the depth penetration of our seismic profiles.

4.3. Algero-Balearic Abyssal Plain Southeast of Ibiza Channel

Lines L026 1010 and L027 1010 (Fig. 11), in the Algero-Balearic Abyssal Plain, display the acoustic stratigraphy of a circular structure west of the NW-SE trending scarp. Line 026 (Fig. 11A) cuts across the structure in an east-west direction with its western end terminating on the eastern flank of the N-S trending high east of the Mar Menor Slope. Sediments east of the circular structure are gently warped; the circular structure is a complex of intrusives (See Section 6.3 in Discussion for the origin of these structures) with maximum reliefs of about 35 m (assuming a velocity of 1500 m/sec). The sediments between the structure and the N-S high east of the Mar Menor Slope are folded, faulted and intruded and the high consists of reflective material that provides no information as to its internal structure. At its base is a narrow

faulted furrow. At Line L027 (Fig. 11B) the circular structure consists of faulted tightly folded uplifted blocks and intervening narrow basins. A basin at the northwest end of the profile is divided in two by a faulted intrusive displaying evidence of bedding. The segment of the basin northwest of the intrusive is divided in two by an unconformity with the strata above it being horizontal. The stratum southeast of the intrusion also is divided in two by an unconformity with the beds above it being horizontal. A narrow body having seafloor expression intrudes the two sequences.

4.4. Mazarrón Escarpment and the adjacent oceanic Algero-Balearic Basin.

The morphology displayed by the Mazarrón Escarpment west and east of the ramp at 0˚30'W in the Mar Menor Margin is reflected in its composition and acoustic stratigraphy. The presence of the Seco de Palos Seamount along its crest suggests that, in contrast to the scarp segment west of the ramp that consists of Bétic Internal Zone rocks, that east of the ramp may consists of a mixture of Internal Zone Bétic rocks and volcanics. A seismic line recorded by Comas et al. (2000) west of the ramp on the upper part of the Mazarrón Escarpment only displays an acoustic gullied unit having acoustic basement characteristics, whereas a seismic line east of the ramp displays two seismic units with average thickness 150 and 100 ms respectively. As described by Comas et al. (2000) the units east of the ramp (volcanics?) cover the gullies in the acoustic basement and are affected in turn by erosion and tectonism. Two lines farther down the scarp, on the uppermost continental rise, on either side of the ramp, display those two units affected by faulting and erosion. A planar fault cutting the units west of the ramp has a seafloor relief of 300 ms (225 m; based on a velocity of l500 m/sec) and another along the west side of the spur at the base of the scarp has a relief of 600 ms (450 m).

Along Profile 051 (Fig. 9B), east of the San Pedro Basin, is a NW-SE trending scarp that cuts across the continental rise. The scarp lacks stratification throughout much of its slope. Sediments at the foot of the scarp are faulted and folded with those at the base of the scarp displaying evidence of uplift, an uplift that is due to motion along the scarp. Warping of sediments in the abyssal plain is probably due to intrusion (See Section 6.3 in Discussion for the origin of these structures)**,** with a low between the warped sediments and the uplifted sediments at the foot of the scarp being filled by horizontal strata. Along Line 049 (Fig.9C), the eastern end of the scarp (SE extension of the Don Juan Fault Zone), consists of an asymmetrical hill whose steep south side is dominated by hyperbolic echoes. Sediments at its base display an acoustic signature suggestive of mass wasting, beyond which the stratified sediments are disrupted by a faulted-furrow and are slightly warped. Along the gentler north side of the hill the sediments extending to near its crest are warped and faulted. Apparently the hill is a block that is tilted northward, a tilting supported by the reversal in dip on the other side of the block farther north.

The northeast-southwest trending line TDS4-L026 (Fig. 12A) off the N-S trending high east of the Mar Menor Slope, shows that the high has an irregular surface and displays acoustic basement characteristics. At the base of the high, at a depth of 3.5 seconds, is a sediment mound about 0.025 seconds thick. Farther south is a multi-peak intrusion, in the abyssal plain, rising 0.075 seconds (56 m) above the seafloor. Line 009 (Fig. 12B), trending somewhat more northerly than line TDS4-L026 displays a pinnacle at the NE end of the profile that could be of igneous origin. This profile also displays acoustic transparent sediment mounds at the base of the north-south high. An acoustic transparent unit in a narrow trough separates the transparent mound from the high. At the southwest of the profile is a faulted sequence cut by a faulted furrow.

The lines in Fig. 13 image the stratigraphy of the Algero-Balearic Abyssal Plain abyssal plain from slightly east of 0˚4'E to 0˚, crossing the 50 km long northeast trending ridge extending from 0˚23'E to 0˚11'W and an ellipsoidal structure north of the ridge. At the northern end of Line TR L5-L6 (Fig. 13A) the ellipsoidal structure consists of two intrusives with reliefs of 35 and 40 m separated by a syncline that has seafloor expression. The ridge consists of an asymmetrical intrusive with a relief of 58 m. Between the ridge and the ellipsoidal structure is a syncline that also has seafloor expression. Along the south side of the ridge is a rim syncline and south of it the abyssal plain sediments are warped and disrupted by fault-controlled furrow with a maximum relief of nearly 0.025 seconds (18.75 m; assuming a velocity of 1500 m/sec).

One of the most enigmatic features mapped during the present investigation is a zone of complex topography at the base of the Mazarrón Escarpment west of the ramp at 0˚30'W. Lines 021 and 022 in Fig. 14 and lines 024 and 026 in Fig. 15 are oriented NW-SE and NE-SW. The northwest end of Line 021 is the southeast end of the spur oblique to the Mazarrón Escarpment, and crosses a channel next to the spur and a field of circular depressions southeast of the channel. The spur is mantled by strata dipping southeastward, the channels has a flat-bottom and is bordered on the southeast by a high, which we infer is an intrusive. The low beyond the intrusive may be one of the circular depressions crossed by the line. To the southeast is another similar depression. Most of Line 021 displays a somewhat irregular seafloor consisting of some highly reflective material. The acoustic nature of the seafloor along Line 022, located in the center on the irregular terrain, is different from that in 021. The topography displayed by this profile is a chain of flat to slightly convex topped highs separated by surfaces dipping to the northeast. There is some suggestion that horizontal strata cap the highs. Southwest of this terrain is a 75 m high intrusive. The

seafloor SW of the intrusive displays undulations either current induced or due to mass wasting.

A different type of acoustic signature is displayed by Line 026-1111 (Fig. 15A). The terrain along this profile has the appearance of a field of folds, the highest of which has a relief of 75 m. The seafloor to the NW of the highest structure is a zone dominated by low relief hyperbolic echoes and to its SE is a zone suggestive of bottom current activity or mass wasting. At the NW end of the profile is the distal end of a fan at the base of the Mazarrón Escarpment. The 3D bathymetry in Fig. 4B indicates that these features are low relief ridges parallel to the Mazarrón escarpment, features that extend to the ramp at 0˚30'W that cuts the Mazarrón Escarpment nearly in two. Line 024-1111 extending southwestward from the base of the Mazarrón Escarpment (Fig. 15B) images the channel at the base of the scarp, a folded multi-peaked high along the southwest side channel and a high relief hummocky terrain into which are cut two pot-holes by turbidity currents.

An oblique view of the rough terrain crossed by the profiles in Figs. 14 and 15 is provided by the 3D bathymetry in Fig. 4B. This image illustrates the continental rise meandering channel extensions off Tiñoso, Cartagena and Palos canyons on the Mazarrón Escarpment, the channel eroded on the spur with its tributaries at its northwest end and the rough terrain cut by the channels. The sharp change in the course of the channel off Palos Canyon from NE-SW to E-W is due to differential erosion along the base of the Mazarrón Escarpment. No evidence of intrusion is displayed by the 3D within the rough east of the spur indicating that intrusion did not play a role in the formation of the rough terrain. Two of such features only occur west of the spur. This rough terrain fronts an embayment in the Mazarrón Escarpment. Highs within the rough terrain display a complex of geometries from linear, highs with spur like projections to short lobes. Cut into this terrain are channel extensions of the

canyons on the Mazarrón Escarpment with the course of one the channels (Fig. 4B) being constricted by a structure paralleling the base of the Mazarrón Escarpment. Similar rough terrain also occurs along the north side of Águilas Canyon cutting the NW trending Palomares Escarpment that joins the Mazarrón Escarpment at about 1˚15'W. This terrain consists of flat-top blocks separated by steep slopes.

Line 007 (Fig. 16) displays the acoustic nature of the spur oblique to the Mazarrón Escarpment. The high is cut into three highs by channels originating at the northwest of the spur (Fig. 4B). The spur's southwest segment is a flat-topped horst tilted to the northeast whose top is mantled by strong reflecting sediments. The other two segments of the spur are sharp peaked and display an acoustic basement signature. Rising above the surface of the abyssal plain are five intrusives, one of which rises a few meters above its surface, and the other rise from 38 to 98 m above it. The channels between them are filled with an acoustic transparent unit.

5. Seismicity

The eastern margin of the Bétic Internal Zone is one of the most seismically active areas in the Iberian Peninsula. Historical events have been documented since the 1500s to present day (Silva et al., 2004). An example of such activity was the 1829 earthquake (Ms of 6.3-6.9) that destroyed the town of Torrevieja (Silva et al., 2004) (Fig. 17). Seismic activity in the splay is associated with the WSW-ENE Crevillente, W-E Bajo Segura, and the NW-NE San Miguel, Torrevieja and Guardamar faults (Alfaro et al., 2002a, 2002b, 2012). About 90 percent of the events have depths of less than 15 km with most of them having magnitudes of less than 4.0 m_b. Earthquakes on land display two trends, a wide band oriented NE-SW and a narrower one on the seaward extensions of the San Miguel, Torrevieja and Guardamar faults that trend NW-SE (Fig. 17). Off Santa Pola, the offshore epicenters display two orientations,

northeast of Santa Pola and ENE-WSW to E-W east of Santa Pola (Fig. 17). The latter trend is associated with the Tabarca-Alicante anticlines whose folds trend in this direction. Some epicenters show clear relationships with active structures offshore (Fig. 17) as the eastern prolongation of the blind thrusts of Tabarca and Alicante. Other seismicity locations are associated with NW-SE transpressive structures shown in Fig. 18. According to Mauffret (2007) these compressive structures extend into the Elche (Alicante) basin north of Tabarca-Alicante as far north as Ibiza Channel. An event (4 of Alfaro et al. 2002b) within the Tabarca-Alicante anticlinorium that we infer is on the seaward extension of the Bajo Segura fault (Fig. 17), with a magnitude of 3.8 mb and depth of 4 km, has a solution with an ENE-SSW trending possible plane, compatible with the fault trends displayed in Figs. 17 and 18.

Similar ENE-WSW seismicity locations also occur south of Tabarca anticlinorium in the San Pedro Basin. Several events south of the Sierra de Cartagena-La Unión also are associated with the Mazarrón Escarpment indicating that the scarp is tectonically active. One event, slightly north of 37˚20'N and slightly east of 0˚50'W is associated with the spur oblique to the Mazarrón Escarpment, further indication that this high is tectonically active. The seven events south the Sierra de Cartagena-La Unión on the Mazarrón Escarpment are in the area of complex topography that may have been formed by gravitational tectonics and the two events slightly west of 0˚30'W are in the rough terrain at the base of the scarp suggesting that seismicity may have played some role in its formation. The other three events west of 0˚ are in the Algero-Balearic Abyssal Plain.

5.1. Focal mechanisms and stress inversion

Eleven focal mechanisms, calculated from Moment Tensor Solution – MTS- (Dziewonski et al., 1982; Stich et al., 2006; Rueda and Mezcua, 2005), have been

analyzed in order to constraint the kinematics and dynamics of the area, and to correlate with active faults (Table III and Fig. 17). The main advantage of focal mechanisms calculated from MTS is their higher reliability, especially if double-couple components of the moment tensors are taken into account Dziewonski and Woodhouse, (1983) Olaiz et al., (2009). Analyzed focal mechanisms show a focal depth shallower than 15 km, and magnitudes (Mw) between 2.7 and 4.8. Most of them are oblique mechanisms (5 compressive-strike slip and 3 extensional-strike slip), 2 correspond with pure strike slip and one is compressive. Five onshore focal mechanisms are located along ENE trending faults (i.e. Crevillente fault), one near San Miguel Fault and one in the north of the Don Juan Fault Zone. Offshore focal mechanisms are transpressive (2), strike-slip (1) and compressive (1). A transpressive focal mechanism is located on the eastern continuation of the E-W Tabarca anticline, and the other three are located eastwards, with a NE-SW direction along the Don Juan Fault Zone (Fig. 17). These focal mechanisms are compressive and strike-slip types.

To calculate the active stress tensor in the zone, a stress inversion procedure (Reches et al., 1992) has been applied to the entire population of earthquakes, as well as to offshore and onshore populations separately (Fig. 17). In both cases the stress tensor obtained has a strike-slip regime (stress ratio of 0.35) with S1 close to N-S and S3 E-W (S2 vertical). Under this stress regime NW-SE faults are right-lateral strike-slip with a reverse component, and NE-SW faults move as reverse with a left lateral component. Under these conditions the E-W earthquake concentration at the Tabarca anticlinorium's should act as a thrust area, supporting Alfaro et al. (in press) thesis. Mechanisms located further east are explained by the movements of NW-SE right lateral faults with a reverse component.

Finally the only focal mechanism located in the south lies in Sierra de La Unión-Cartagena is a compressive mechanism and compatible with the thrust front of

this Sierra. No conclusive data permit us to discriminate the current tectonic activity of the Mazarrón Escarpment, but the E-W direction is compatible with right lateral movement, without excluding gravitational processes. The few earthquakes located at the Mazarrón Escarpment agree well with the GPS displacements (Serpelloni et al., 2007; Pérez Peña et al., 2010) as well as the model of Alfaro et al. (2002a; 2012). All seismicity data support Alfaro's et al. (2002b) thesis of an actual NNW-SSE compression under a strike-slip to compressive stress regime at the eastern end of the Bétic System, and that this system extends offshore.

6. Discussion

In this section of the paper we bring together all the data on the geomorphology and high resolution seismic data to reconstruct the geologic setting of the offshore extension of the Bétic System. Our objective is to determine whether similar or different tectonic processes form the onshore and offshore segments of the Bétic System and if they are different how and why they are different. We infer that the quality acquired during this investigation allows us to do this.

The 3D bathymetry constructed from multi-beam data recorded during the present investigation coupled with high-resolution TOPAS seismic reflection profiles have provided images of the Algero-Balearic basin and adjacent margins comparable to that of the photogenic perception of subaerial topography and geology. The area has a complex morphology, resulting from the interaction of surface and deep processes, within a tectonic NW-SE convergence between Africa and Iberia. Surface processes offshore include: a) the impact of Pleistocene glacially induced transgressions/regressions, b) present day modern currents molding the surface of the continental shelf, b) development of large-scale field of pockmarks formed by the expulsion of gas/water, and c) the mass wasting on the Mazarrón Escarpment caused

by sediment loading and stresses associated with the Africa-Iberia convergence. Depth processes including: a) the presence of an important recent volcanism inshore and offshore, b) the extensive field of salt diapirs with their surrounding synclines in the Algero-Balearic Abyssal Plain and evaporites in the coastal basins (Riding et al., 1998), and c) a distributed deformation, including brittle and ductile structures, acting in response to the Africa-Iberia convergence, which is responsible for the present-day seismicity.

6.1. Offshore Extension of the Bétic Internal Zone

The present and previous investigations clearly demonstrate that the deformation of the onshore upper Miocene-Quaternary in southeast Spain associated with the terminal splay of the Eastern Bétic Shear Zone continues offshore. This compression, driven by the convergence of the African and Eurasian plates, for example, formed the 80 km long, 20-30 km wide Tabarca anticlinorium north of Mar Menor. This tectonic deformation is also responsible for the extensive volcanism in the Mar Menor lagoon, shelf (Isla Grosa group and the Hormigas Islands), and San Pedro Basin (offshore extension of the coastal Murcia basin), east of Mar Menor. Volcanism is in the form of seamounts and pinnacles. Morphologically the pinnacles resemble dikes off Cape Verde Islands off the west coast of Africa (Emery and Uchupi, 1984). The volcanics and dikes in the region range in age from the Miocene to the Pleistocene. Seismicity is present throughout the region with focal depths being shallower than 15 km, the magnitudes ranging between 2.7 and 4.8. Most focal mechanisms belong to compressive to strike-slip stress regime. Many faults extend to the seafloor with some of them serving as passageways for the expulsion of gas/fluids and the creation of pockmarks. These faults may be the surface expression of much deeper and larger structures in the basement. Along the southern side of the Bétic

Shear Zone, defined by the Sierra de Cartagena-La Unión, the NW-SE trending transcurrent faults in the coastal area are related to recent tectonic events involving strike-slip and compression. Seismic activity associated with the transcurrent faults that extend across the Sierra de Cartagena-La Unión shelf to the Mazarrón Escarpment, is responsible for the Holocene mass wasting and turbidity current activity on the scarp. Seismic reflection profiles recorded on the Sierra de Cartagena-La Unión Shelf also indicate that the Paleozoic, Permian and Triassic metamorphic complexes of the Internal Bétic Zone of the Sierra de Cartagena-La Unión extend across the shelf on the subsurface to the Mazarrón Escarpment. Whereas the eastern extension of the Bétic system has a thick Miocene-Quaternary cover, the system in the Sierra de Cartagena-La Unión Shelf is only thin sediment veneer, so thin as to be imaged in our low energy TOPAS seismic reflection profiles. Only the western end of the shelf is the sediment thick enough so that the Bétic system is too deep to be imaged in our profiles.

6.2. The Mazarrón Escarpment

The most prominent feature displayed by Fig. 18 is the 1,800 m high, 7 to 19 km wide and 145 km long Mazarrón Escarpment with a gradient that ranges from 14˚ to 31˚. Its crest ranges from 2,400 m at its eastern end to 225 m south of the Mar Menor Shelf, 112-149 m at 0˚45'-1˚15'W off the Sierra de Cartagena-La Unión and 675 m at 1˚ 24'W. These depths indicate that the scarp is warped along its strike, a warping that may result from differential transcurrent/transpression movement along the strike-slip faults that are orthogonal to oblique to the scarp. This scarp, together with the Emile Baudot Escarpment to the east are first order morphologic features forming the boundary between two mega-structural elements of the region, the Bétic System and the oceanic Algero-Balearic Basin. It has been proposed that the Alborán

microplate, forming the foundation of the Alborán Basin west of the Algero-Balearic Basin, migrated westward along the right lateral fault Emile Baudot fault (Vegas, 1992; Acosta et al., 2001a; Fig. 1). The presence of cataclastic fine-grained breccias composed of slates and carbonates at its base (Fernández-Soler, 2000a) suggests that the Mazarrón Escarpment also has the same origin. If such a migration took place along the Mazarrón Escarpment it is not reflected in its morphology. However, the Mazarrón Escarpment is not the only transform that lacks topographic irregularities. The Ivory-Ghana Ridge, in the Gulf of Guinea, along which South America separated from Africa, for example, also lacks topographic irregularities created by this continental separation (Emery and Uchupi, 1984).

The western end of the Mazarrón Escarpment is at 1˚18'W where the trend of the scarp changes from E-W to NW-SE (Palomares Escarpment), a change marked by slumping at the base of the scarp. Mazarrón Escarpment rapidly loses its relief east of 0˚09'E, but still has a height of several hundred meters at 20'E where it terminates abruptly along the west side of a north-south trending channel. Like the Emile Baudot Escarpment, there is no evidence of the Mazarrón Escarpment within the 60 km wide southeastern approach to the Ibiza Channel. Apparently the Ibiza Channel separating the Balearic Promontory from the Mar Menor Margin is a major structural discontinuity. The topography within this structural terrane is complex consisting of two right-lateral NW trending strike-slip faults which we have named the Don Juan Fault Zone (Fig.17), reverse faults, anticlinoriums, seamounts, mud volcanoes, pockmarks formed by the extrusion of gases/fluids and possibly diapirs with cores of Messinian evaporites. Possibly the channel is the creation of a change in the direction of migration of the Alborán plate from NE-SW, the trend of the Emile Baudot Escarpment, to E-W, the trend of the Mazarrón Escarpment.

The northwest-southeast 10 by 20 km spur oblique to the Mazarrón Escarpment at about 0˚40'W is bounded by high-angle normal faults with the one on the west side of the spur, the Tiñoso Fault, having a relief of 600 ms (or 450 m assuming a velocity of 1500 m/sec; Comas et al. (2000); Marro et al. (2006). Similar features at the southern end of the Emile Baudot Escarpment were inferred by Camerlenghi et al. (2009) to be of volcanic origin. Seismic profiles (Fig. 16) indicate that the high is a horst oblique to the scarp, and dredge samples indicate that is not volcanic. A dredge sample from the tip of the horst consisted of three rounded clasts and some coral rich-crust pieces (Fernández-Soler et al., 2000a). The lithic fragments consisted of carbonate covered by corals that overlie orthogneiss. Fernández-Soler et al (2000 a,b) correlated the carbonate clasts with the Bétic Internal Zone in the Cartagena area. They also stated that the only lithology comparable to the granitoids is the isolated plutonic pebble zenoliths in the Cabo de Gata Miocene volcanics. We have no data as to how the spur came into existence, but is probably the consequence of pure strike-slip or transpressive motion along the Mazarrón Escarpment. Possibly the spur is a divergent splay formed by a minor change in the strike of the scarp of Mazarrón. Harding et al. (1985) has described such structures along a plate boundary where it bends or splays. An alternative explanation for the spur and the massive collapse of the Mazarrón Escarpment east of the spur may be due to motion along the strike-slip faults extending across the Sierra de Cartagena-La Unión shelf to the crest of the scarp (Figs. 17 and 18), at 0° 33'E.

Another possibility is that the spur is an allochthonous block, comparable to the Rio Grande del Norte off northeast Brazil (Emery and Uchupi, 1984 and references therein), which became attached to the Mazarrón Escarpment as the Alborán plate migrated westwards.

The Mazarrón Escarpment displays distinct tectonics and morphologies features east and west of a ramp that cuts the scarp nearly in two at 0˚30'W (Figs. 1B and 2A). West of the ramp the top of the scarp is cut by one NW trending and one nearly EW trending right lateral faults and one NE trending left lateral fault (Figs. 17 and 18). The canyons west of the ramp also appear younger than those east's of the ramp, and their heads are located at or near the shelf's edge. A seismic line recorded by Comas et al. (2000) west of the ramp of the Mazarrón Escarpment only displays gullied unit having acoustic basement. Another seismic reflection profile recorded by Marro et al. (2006) on the upper part of the Mazarrón Escarpment immediately west of the ramp images a faulted, thin, well-bedded sequence resting on acoustic faulted basement. From 1˚W to the western edge of the survey area at 1˚30'W the upper part of the Mazarrón Escarpment is covered by a prograding sediment wedge whose base ranges in depth from 113 m on the east to 675 m on the west. Its surface is smooth and not cut by gullies. East of the ramp, the upper part of the Mazarrón Escarpment is cut by three parallel NE trending left-lateral faults, the Seco de Palos fault zone (Figs. 17 and 18). Two of these faults extend the width of the Mazarrón Escarpment. Acoustically, the scarp east of the ramp displays two seismic units with average thickness 150 and 100 ms respectively that are affected by erosion and tectonism. The presence of Seco de Palos Seamount (or Palos Seamount) along the crest of the scarp, that is nearly cut in two by one of those gullies eroded along a left-lateral fault of the east of north trending Seco de Palos fault zone (see Fig. 17), indicates that part or all of the two seismic units consist of volcanics. As described by Comas et al. (2000), these units that cover the gullies cut in the acoustic basement that probably represents the Bétic Internal Zone in the Mazarrón Escarpment. Two lines on the uppermost continental rise south of the scarp, on either side of the ramp, display those two units affected by faulting and erosion. Such deformation also is imaged by the multi-beam

bathymetry and the seismic reflection profiles we recorded seaward of the Mazarrón Escarpment.

The absence of a continental rise and their more subdued topography (Fig. 4A), suggest that the canyons east of the ramp are not presently active. Their narrow sharp crested divides, evidence of mass wasting at their heads and continental rise channel extensions, suggest that the canyons west of the ramp at 1˚06'W are active today. Such mass wasting has led to the massive collapse of Mazarrón Escarpment creating a 27 km wide embayment centered at 0˚40'W (Figs. 4B and 18). At the foot of the embayment is a 47 km by 33 km slide deposit involving Quaternary and Late Pliocene sediments displaying a chaotic topographic geometry of ridges, faulted blocks bound by high angle faults and folded massifs that are cut by channel extensions of the canyons on the Mazarrón Escarpment (Figs. 14-15). If this slide is the Cartagena Slide described by Comas and Ivanov (2006), then its area is much larger than the one estimated by them. They stated that it had an area of several sq. km whereas our data suggests that it has an area of at least 1035 sq. km. Both data sets confirm Woodside et al. (2000) conclusion from analyses of side-scan data indicating that the Mazarrón Escarpment west of the ramp centered at 0˚30'W, has undergone or is undergoing massive wastage by gravitational processes. We infer that the slide probably occurred as a result of activity along a NW-SE strike fault that can be traced across the Sierra de Cartagena-La Unión Shelf to its outer edge (Figs. 3C and 17). Another massive failure also occurs in the area of Águilas Canyon, cut into the NW trending Palomares Escarpment (Fig. 18). This structure consists of a series of fault bound blocks in trough flanked by a flat-top high to the south and the NW trending Palomares Escarpment. Águilas Canyon was cut along the contact between the slide and the flat-top high subsequent to the slide.

Erosion of the Mazarrón Escarpment probably took place during three distinct episodes. The earliest was during the Messinian regression and desiccation of the Mediterranean 5.6-5.3 Ma, when sea level dropped over 2000 m in the Mediterranean Sea (Meijer and Krijgsman, 2005). It is at this time that the gullies on the Mar Menor Slope and adjacent highs (Figs. 1A and 2A) were fluvially eroded to create "badland" topography. It is at this time that evaporites were deposited in the deep basins (Clauzon et al, 2011; García et al, 2011; Lofi et al., 2005; Maillard et al., 2006; Rouchy and Caruso, 2006; Ryan, 1978; Ryan and Cita, 1978). Possibly it was at this time that the scarp east of the ramp was mantled by volcanic sediments, but we have no data to verify this.

During and subsequent to the Zanclean flood the upper parts of the canyons east of the ramp and the heads of those west of the ramp from 1˚06'W to the western edge of the survey area at 1˚30'W were buried by Plio-Quaternary sediments; possibly the canyons immediately west of the ramp to 1˚06'W remained exposed. The scarp underwent a second cycle of erosion (Pliocene?/Early Pleistocene?) during which the volcanic and sediment cover on the canyons east of the ramp was eroded.

A third erosional cycle took place during the glacially induced regression in Late Pleistocene when sea level dropped to about 120 m below its present level. This erosional cycle only affected the canyons immediately west of the ramp; the heads of the other canyons are too deep. The canyons east of the ramp and those west of 1˚06'W are inactive today, whereas those immediately west of the ramp to 1˚06'W are active and are serving as pathways for sediments onto the continental rise and abyssal plain. This difference is a consequence of sedimentary processes taking place on the adjacent shelf today and recent tectonism associated with the faults extending across the shelf.

The eastern Sierra de Cartagena-La Unión Shelf is covered by an extensive field of sediment waves trending obliquely to the shore, the creations of west flowing currents. The heads of the canyons indenting the shelf are trapping some of these westward moving detritus. With continuous accumulation, the sediments at the heads of the canyons become unstable and move down canyons to the deep-sea, leading to mass wasting at their heads, erosion along their axes, formation of channels on the continental rise and inter-channel turbiditic deposits with their undulating surfaces created by the turbidity currents that overflow the channels. Tectonic activity along the transcurrent faults extending across the shelf to the Mazarrón Escarpment also must have contributed to the mass wasting and turbidity currents on the canyons. Several of the offshore seismic events are associated with the Mazarrón Escarpment indicating that the scarp is tectonically active.

6.3. Salt Structures

The 3D bathymetry in Fig. 4A, the seismic reflection profiles in Figs. 11-13 and the morpho-tectonic map in Fig. 18 image numerous single to multiple peak structures rising 10's of meters above from the seafloor of the Algero-Balearic basin. Although no evaporites have been sampled in any of these structures to date (Bobrov, 2000; Fernández-Soler et al., 2000a), it is geologically reasonable to infer that these relief features could be related to the plastic flow of the Messinian evaporites below the Plio-Quaternary sediments. The Messinian evaporites in the western Mediterranean consist essentially of halite, a material that can deform in a plastic manner leading to gravity spreading and/or gliding of the halite and the sediments above (Gaullier et al. (2010). The basin provides the gravity instability slope along which are three domains: extensional domain up slope, a translation domain on mid slope and a contractional domain (salt anticlines, diapirs, thrusts) down slope (Vendeville, 2005). Gaullier et al.

(2010) and Maillard et al. (2003) have further pointed out that structural trends within the glided formations mimic the trends in the formations beneath the salt décollement. Brun and Fort (2010) stated that from a theoretical point of view, gliding on any basal slope, not matter how small, is more efficient than sediment loading in creating salt diapirism. Yet the question remains is the gradient on an abyssal plain, probably measured in minutes, is too small to trigger such gliding of the sediments over the salt. According to Gaullier et al. (2010), such tectonics slows or stops when the general slope decreases. In such case, gravitational salt tectonics in a structure, such as the Algero-Balearic Basin, would be restricted to its margins with the driving force in the center of the basin being sediment loading. Lack of penetration of our seismic reflection profiles makes it impossible to discern whether the structures displayed by our profiles in the Algero-Balearic Basin are the result of gliding caused by uplift along the Mazarrón Escarpment, sediment loading or regional folding due to the convergence of the Eurasian and African plates as proposed by Mauffret (2007). However, our data do indicate that the structures have a higher concentration in the direction of the Mazarrón Escarpment and diminished in number toward the center of the basin and against the scarp (Fig. 18). Thus, some of the diapirs could be due to uplift along the scarp.

Stanley et al. (1974) have demonstrated that the salt structures continue through Horizon M, the top of the Messinian evaporites, and that the horizon is deformed by the diapirs. Our data does show that the diapiric structures in the Algero-Balearic Basin south of the Mazarrón Escarpment are not evenly distributed through the abyssal plain and that they are separated from the escarpment by a narrow strip of undisturbed seafloor. Our data also indicate that the structures have a higher concentration in the direction of the Mazarrón Escarpment and diminished in number toward the center of the basin and against the scarp (Fig. 18).

The morphology of the salt diapirs ranges from elongate ridges trending northeast, ellipsoid-shape with a central syncline, “Y” shaped mounds or single isolated diapirs of sub-circular shape. The deformed strata along the NW trending scarp in Fig. 9B-C may represent salt walls formed along normal faults in the overburden in the manner described by Jackson and Vendeville (1994). The walls south of the Mazarrón Escarpment may mimic structural trends in the layer beneath the salt as described by Gaullier et al. (1993) and Maillard et al. (2003). If these features do mimic the structural trend of the layers beneath the salt, these trends may represent divergent wrench structures associated with the transcurrent-transpression motion along Mazarrón Escarpment as the Alborán microplate migrated westward. According to Harding et al. (1985) such divergent styles occur along transform systems, such as the Mazarrón Escarpment, where the displacement zone bends or splays.

Reliefs of the diapirs are from several to 75 meters and the shapes of their crests varied from sharp peaks to rounded ones. The structures occurs as individual peaks to a complex of several structures separated by synclines (Figs.12-13). In some of the synclines associated with the diapirs, the dips of the folded sediments increase below the surface. Stanley et al (1974) infer that this is either due to an upward decrease in subsidence or a progressive increase in sedimentation. Unconformities within the synclines also indicate that synclinal formation was episodic. Whereas, some of the synclinal structures have seafloor expression, in others horizontal strata fill the synclinal lows form the abyssal plain. Stanley et al (1974) proposed that this abrupt termination in synclinal formation is due to local deposition exceeding deformation. Anticlinal structures bounded by faults having seafloor expression also are commonly associated with the diapirs. Warping adjacent to the faults is probably

due to drag, but Stanley et al. (1974) has pointed that such warping could also be due to local compaction caused by the release of interstitial fluids.

Where sedimentation and salt movement are coeval, the stratal geometry is different from that in the Algero-Balearic Basin. In the La Popa Basin, Mexico, for example, the rise of the El Gordo diapir influenced depositional patterns in the vicinity of the salt structure. A siliciclastic apron onlap and thin toward the diapir, there are progressive unconformities proximal to the diapir, carbonate lenses occur next to the diapir and diapiric derived metamorphic clasts occur within the carbonate lenses (Mercer and Giles, 2005). The carbonate lenses are thicker next to the diapir and their deposition was influenced by the relief of the diapir. The carbonate reefal facies are underlain by debris lows generated by the diapiric rise that caused its slope to fail.

The most unusual structure mapped within the diapiric field during our investigation is a circular structure west of the scarp cutting obliquely across the Algero-Balearic Abyssal Plain. The structure, with a diameter of 14 km, located east of the Mazarrón Escarpment (Figs. 2B, 11 and 18), consists of diapirs separated by folded and uplifted sediments (Fig. 11). The structures are located on a circular basement low, in a basement map compiled by Mauffret (2007, his Fig. 3). Lack of penetration in our seismic profiles makes it impossible to discern the cause of the association between the basement low and the diapirs. Possibly the diapirs are a reflection of the morphology of the basement around the perimeter of the depression. Possibly the faulted furrows west and northwest of the circular structure that circumscribe the low also reflect the configuration of the basement beneath the salt. Structures having the same trends were formed by Maillard et al. (2003, their Fig. 9) in a physical experiment where silicone was used to represent the halite. In their model, tilted 3˚, differential compaction of pre-Messinian sediments over a basement step transmitted the dormant fault controlled basement step into the evaporites creating features

comparable to the furrows 3 hours later. Except in their model the look-alike features are folds and the features in Fig. 18 are horsts.

6.4 Shelf Micro-topography

The shelf surface is defaced by bottom current generated structures; relict features formed during the Holocene transgression and small islands rocky ledges of volcanic origin northeast off Cabo de Palos and the low relief Hormigas and Grosa islands. López- Ruiz et al. (2002) inferred that this volcanism is due to an increased in the rate of convergence of the African and Eurasian plates from latest Miocene to the present. Superimposed on the shelf's surface are linear ridges and between them a wide expense of sediment waves oriented obliquely to shore with their steep slopes facing southeastward. We interpret those ridges as former barrier islands. The bars appear to consist of some strong reflecting sediment, possibly carbonates in the form of dunes, which mask the sediments beneath them. Possibly, the stratified sediment northwest of the bars represents lagoon sediments. The sediment drifts between the barrier islands are being formed today by southwest flowing current known as the Liguro-Provençal-Catalán Current or North Current. Some of the sediments transported southward by the North Current are trapped by the east-west trending Torrevieja half-graben and then transported eastward into the deep-sea.

7. Conclusion

The seismically active southeastern Iberian continental margin, the seaward extension of the eastern end of the Bétic System, is the creation of the convergence of the African and Eurasian plates from Late Oligocene to the present, a convergence that has varied in intensity and direction with time. Newly acquired multi-beam bathymetry and high resolution seismic reflection profiles, at a density not available to

date, has made possible for us to map the morpho-tectonic fabric of this margin in detail. We not only mapped the primary geomorphic features of the southeastern Spanish margin, but also the distribution and geometry of such secondary features as seamounts and pinnacles, pockmarks due to the expulsion of thermogenic fluids and gases, folds and reverse and right/left lateral faults, bars formed during the Holocene transgression on the shelf surface east of Mar Menor, and recent sediment drifts created by the southern flowing Northern Current on the shelf. These data also provided detailed information on the morphology of the Mazarrón Escarpment separating the Bétic Zone from the oceanic Algero-Balearic Basin, a morphology created by a combination transcurrent faulting, turbidity current erosion and mass wasting probably triggered by recent seismic events, events that are scattered throughout the margin. The sediments of the Algero-Balearic Basin, an oceanic basin formed by the western migration of the Alborán plate along the Mazarrón Escarpment in Middle Miocene, are deformed by the plastic flow of Messinian evaporites. This diapirism could be the consequence of a combination of gliding of Pliocene-Quaternary sediments atop Messinian halite, uplift along the Mazarrón Escarpment, sediment loading and convergence of the African and Eurasian plates.

Acknowledgements

We thank officers and crew of R/V Vizconde de Eza and R/V Emma Bardán (General Secretariat of the Sea – SGM) for their effort during the cruises to the Spanish southeast margin, as well as members of the Spanish Oceanographic Institute (IEO) who participated in the various cruises. The Cartography Group SGM-TRAGSA participated in the different cruises and processed the multi-beam data. Thanks also are due to Andrew Bell, associate editor, Agnès Maillard and an anonymous referee. Their

constructive comments were of considerable help in revising and improving the manuscript. This is a contribution to Capesme and Espace Projects, which are funded by IEO in collaboration with SGM.

References

Acosta, J., Muñoz, A., Herranz, P., Palomo, C., Ballesteros, M., Vaquero, M., Uchupi., 2001a. Geodynamics of the Emile Baudot Escarpment and the Balearic Promontory, western Mediterranean. Marine and Petroleum Geology 18, 349-369.

Acosta, J., Muñoz, A., Herranz, P., Palomo, C., Ballesteros, M., Vaquero, M., Uchupi, E., 2001b. Pockmarks in the Ibiza Channel and the western end of the Balearic Promontory (western Mediterranean) revealed by multi-beam mapping. Geo-Marine Letters 211, 123-130.

Acosta, J., Ancochea, E., Canals, M., Huertas, M. J., Uchupi, E., 2004. Early Pleistocene volcanism in the Emile Baudot Seamount, Balearic Promontory (Western Mediterranean Sea). Marine Geology 207, 247-257.

Alfaro, P. Andreu, J.M., Delgado, J., Estévez, A., Soria, J.M., Teixidó, T., 2002a. Quaternary deformation of the Bajo Segura blind fault (eastern Betic Cordillera, Spain) revealed by high-resolution reflection profiling. Geol. Magazine 139, 331-341.

Alfaro, P., Delgado, J., Estévez, A., Soria, J.M., Yébenes, A., 2002b. Onshore and offshore compressional tectonics in the eastern Bétic Cordillera (SE Spain). Marine Geology 186, 337-349.

Alfaro P., Bartolomé R., Borque M.J., Estévez A., García-Mayordomo J., García-Tortosa F.J., Gil A., Gràcia E., Lo Iacono C., Perea, H., 2012. Journal of Iberian Geology 38 (1): In press.

http://dx.doi.org/10.5209/rev_JIGE.2012.v38.n1.39217.

Azañón, J.M., Martínez-Martínez, J.M., Rodríguez-Fernández, Sánchez-Gómez, M., Soto, J.I., BASACALB cruise (TTR-9 Leg 3) Scientific Party., 2000.

Extensional structures in the Mazarrón margin and onshore area (Betics, SE Spain). Geological Processes on the European continental margins. International Conference and Eighth Post-Cruise Meeting of the Training-Through-Research Programme. Granada, Spain, 31 January- 3 February 2000, Intergovernmental Oceanographic Commission. Workshop Report No. 168, 30pp.

Azañón, J.M., Galindo-Zaldívar, J., García-Dueñas, V., Jabaloy., 2002. Alpine tectonics II; Betic and Balearic Islands. In: Gibbons, W., Moreno, T. (Eds.). The Geology of Spain. The Geological Society of London, pp. 401-416.

Bobrov, A.M., 2000. The bottom of upper Messinian evaporites observed within diapirs of the South Balearic Basin. Geological Processes on the European continental margins. International Conference and Eight Post-Cruise Meeting of the Training-Through-Research Program Granada, Spain, 31 January- 3 February 2000, Intergovernmental Oceanographic Commission. Workshop Report No. 168, p. 24.

Bousquet, J.C., 1979. Quaternary strike-slip faults of southeastern Spain. Tectonophysics 52, 277-286.

Brun, J.P., Fort, X., 2010. The analysis of salt tectonic systems: Salt Tectonics, sediments and prospectivity. A Research Conference Sponsored by the Petroleum Group of the Geological Society of London and SEPM Society for Sedimentary Geology, 2-22 January 2010. Burlington House, London, UK, p. 15.

Camerlenghi, A., Accettella, D., Costa, S., Lastras, G, Acosta, J., Canals, M., Wardell, N., 2009. Morphogenesis of the SW Balearic continental slope and adjacent abyssal plain, western Mediterranean Sea. International Journal Earth Sciences 98, 735-750.

Clauzon, G., Suc, J.P., Gautier, F., Berger, A., Loutre, M.F., 2011. Alternate interpretation of the Messinian salinity crisis: controversy resolved?. Geology 24, 363-366.

Comas, M., Ivanov, M., 2006. The Palomares and Cartagena margins. Interdisciplinary geosciences studies of the Gulf of Cadiz and Western Mediterranean basins. IOC Technical Series No. 70, UNESCO, 2006 (English), p. 55-56.

Comas, M., Talukder, A., Woodside, J., Volkonskaya, A., 2000. South Balearic Basin: the Palomares and Mazarrón margins. Multidisciplinary Study of Geological Processes on the North East Atlantic and Western Mediterranean Margins. IOC Technical Series No. 56, UNESCO, 2000 (English), p. 91-95.

Conesa, H.M., Jiménez-Cárceles, F. J., 2007. The Mar Menor lagoon (SE Spain): a singular natural ecosystem threatened by human activities. Marine Pollution Bulletin 54, 839-849.

De Mets, C., Gordon, R.G., Argus, D.F., Stein, S., 1990. Current plate motions. Geophysical Journal International 101, 425-478.

Díaz del Río, V., 1993. Estudio Geoambiental del Mar Menor. Monografías del Instituto Español de Oceanografía, 4, 223 pp.

Dziewonski, A.M., Chou, T.A., Woodhouse, J.H., 1982. Determination of earthquake source parameters from waveform data for studies of global and regional seismicity. Journal of Geophysical. Research 86, 2825–2852.

Dziewonski, A.M., Woodhouse, J.H., 1983. An experiment in the systematic study of global seismicity: centroid moment-tensor solutions for 201 moderate and large earthquakes of 1981. Journal of Geophysical Research 88, 3247–3271.

Duggen, S., Hoernle, K., ven den Boaggard, P., Harris, C., 2004. Magmatic evolution of the Alborán region: the role of subduction in the forming of the western

Mediterranean and causing the Messinian crisis. Earth and Planetary Science Letters 218, 91-108.

Duggen, S., Hoernle, K., van den Boggard, P., Garbe-Schönberg, D., 2005. Post-collisional transition from subduction to intraplate-type magmatism in the westernmost Mediterranean: evidence from continental edge delamination of subcontinental lithosphere. Journal of Petrology 46, 1155-1201.

Emery, K.O., Uchupi, E., 1984. The Geology of the Atlantic Ocean. New York, Springer-Verlag, 1050 pp.

Fernández Soler, J., Martinez-Ruiz, F., Akhmanov, A., Stadnitskaya, A., Kozlova, E., Sautkin, A., Mazurenko, L., Ovsyannikov, D., Sadekov, A., Suslova, E., Goncharov, D., 2000a. South Balearic Basin: the Palomares and Mazarrón margins. Bottom Sampling Results. Multidisciplinary Study of Geological Processes on the North East Atlantic and Western Mediterranean Margins. IOC Technical Series No. 56, UNESCO, 2000 (English), p. 98-99, Annexe I, p. 22-25.

Fernández-Soler, J.M., Azañón, J.M., Sánchez-Gómez, M., Soto, J.I., Martínez-Martínez, J.M., BASACALB Cruise (TTR-9 Leg 3) scientific Party., 2000b. Major findings on the nature of acoustic basement rocks in the Alborán and South Balearic basins from BASACALB cruise (TTR-9, Leg 3). Geological Processes on the European continental margins. International Conference and Eighth Post-Cruise Meeting of the Training-Through-Research Programme. Granada, Spain, 31 January-3 February 2000, Intergovernmental Oceanographic Commission. Workshop Report No. 168, p. 31.

Font, J García-Ladona, E., Gorriz, E., 1995. The seasonality of mesoscale motion of the Northern Current on the western Mediterranean. Oceanologica Acta 18, 207-218.

Gallart, J., Vidal, N., Estévez, A., Pous, J., Sábat, F., Santisteban, C., Suriñach, P. and the Valencia Trough Group., 1995. The ESCI-Valencia Trough vertical experiment: a seismic image of the crust from the NE Iberian Peninsula to the western Mediterranean. Revista Sociedad Geológica de España 8, 405-415.

García, M., Maillard, A., Aslanian, D., Rabineau, M., Alonso, B., Gorini, C., Estrata, F., 2011. The Catalán margin during the Messinian Salinity Crisis: physiography, morphology and sedimentary record. Marine Geology 284, 158-174.

García-Mayordomo, J., Martínez-Díaz, J.J., 2006. Caracterización del Anticlinorio del Bajo Segura (Alicante): fallas del Bajo Segura, Torrevieja y San Miguel de Salinas. Geogaceta 40, 19-22.

Gràcia, E., Bartolomé, R., Lo Iacono, C., Moreno, X., Martínez-Loriente, S., Perea, H., Masana, E., Pàllas, R., Diez, S., Dañobeitia, J., Terrinha, P., Zitellini, N., 2010. Characterizing active faults and associated mass transport deposits in the south Iberian margin (Alborán Sea and Gulf of Cadiz): on-fault and off-fault paleosismic evidence. Resúmes de la 1˚ Reunión Sobre Fallas Activas y Paleosismología. Sigüenza, Spain, 163-166.

Gaullier, V., Brun, J.P., Guerin, G., Lecanu. H., 1993. Raft tectonics: the effects of residual topography below a salt decollement. Tectonophysics 228 (3/4), 363-381.

Gaullier, V, Loncke, L., Vendeville, B., Obone Zue Obame, E., Déverchère J, Droz, L., 2010. Interaction betweem salt tectonics and deep-seated tectonivs. Part I; examples from the western Mediterranean. In: Salt Tectonics, Sediments and Prospectivity. A research Conference Sponsored by the Petroleum Group of

The Geological Society of London and SEPM Society of Sedimentary Geology. Burlington House, London, UK, pp. 84.

Harding,T.P., Vieerbuchen, R.C., Christie-Blick, N., 1985. Structural styles, plate tectonic settings, and hydrocarbon traps of divergent (transtensional) wrench faults. In: Biddle, K.T., Christie-Blick, N. (Eds.) Strike-Slip Deformation, and Sedimentation. Soc. Econ. Paleontologists and Mineralogists Special Publication 37, 51-78.

Herraiz, M., De Vicente, G., Lindo-Naupari, R., Giner, J., Simón, J.L., Gonzáles-Casado, J.M., Vadilla, O., Rodríguez-Pascua, M.A., Cicuéndez, J.I., Casas, A., Cabañas, L., Rincón, P., Cortés, A.L., Ramírez, M., Lucini., 2000. The recent (upper Miocene to Quaternary) and present tectonic stress distribution in the Iberia Peninsula. Tectonics 19, 762-786.

Huibregtse, P., van Alebeek, H., Zaal, M., Biermann., 1998. Palaeostress analysis of the northern Nijar and southern Vera basins: constrained for Neogene displacement history of major strike-slip faults in the Betic Cordilleras, SE Spain. Tectonophysics 300, 79-101.

Jackson, M.P.A., Vendeville, B.C., 1994. Regional extension as a geologic trigger for diapirism. Geological Society of America Bulletin 106, 57-73.

Jiménez-Martínez, J., Candela, L., García-Aróstegui, J.L., Aragón, R., 2012. A 3D geological model of the Campo de Cartagena, SE Spain: hydrological implications. Geologica Acta 10/1, 1-14.

Lofi, J., Gorini, C., Berné, S., Clauzon, G., Tadeu Dos Reis, A., Ryan, W.B.F., Stickler, M.S., 2005. Erosional processes and paleo-environmental changes in the western Gulf of Lions (SW France) during the Messinian Salinity Crisis. Marine Geology 217, 1-30.

López-Ruiz, J., Cebriá, J.M., Doblas, M., 2002. Cenozoic volcanism I: the Iberian Peninsula. In: Gibbons, W, Moreno, T (Eds.) The Geology of Spain. The Geological Society of London, 417-438.

Maillard, A., Gaullier, V., Vendeville, B.C., Odonne F., 2003. Influence of differential compaction above basement steps on salt tectonics in the Ligurian-Provençal Basin, northwest Mediterranean. Marine and Petroleum Geology 20, 13-27.

Maillard, A., Gorini, C., Mauffret, A., Sage, F., Lofi, J., Gaullier., 2006. Offshore evidence of polyphase erosion of the Valencia Basin (northwestern Mediterranean): scenario for the Messinian Salinity Crisis. Sedimentary Geology 188-189, 69-91.

Maillard, A., Mauffret, A., 2011. Structure and present-day compression in the offshore area between Alicante and Ibiza Island (Eastern Iberian Margin). Tectonophysics, doi:10.1016/j.tecto.2011.07.007.

Manteca Martínez, J.I., Ovejero Zappino, G., 1992. Los Yacimientos Zn, Pb, Ag-Fe del distrito minero de la Unión-Cartagena, Bética Oriental. In: García Guinea, J., Martínez Frias, J. (Eds.) Recursos Minerales de España. Consejo Superior de Investigaciones Científicas, Madrid (CSIC), pp. 1085-1101.

Marro, G., Sánchez-Gómez, M., Fernández Ibánez, F., García, M., Román-Alpiste, M.J., Vanneste, H., Comas, M., 2006. The Cartagena margin: seismic interpretation. Interdisciplinary geoscience studies of the Gulf of Cadiz and Western Mediterranean basins. IOC Technical Series No. 70, UNESCO, 2006 (English), p. 61.

Mauffret, A., 2007. The northwestern (Maghreb) boundary of the Nubia (Africa) plate. Tectonophysics 429, 21-44.

Mauffret, A., Maldonado, A., Campillo, A., 1992. Tectonic framework of the eastern Alboran and western Algerian basins (western Mediterranean). Geo-Marine Letters 12, 104-110.

Mauffret, A., Frizon de Lamotte, D., Lallemant, S., Gorni, C., Maillard, A., 2004. E-W opening of the Algerian Basin (western Mediterranean). Terra Nova 16, 257-264.

Mercer, D.W., Giles, K.A., 2005. Upper Cretaceous to Lower Paleogene carbonate growth strata associated with a passive salt diapir, La Popa Basin, Mexico: an outcrop analog to shelf salt exploration (Abstract). AAPG Search and Discovery Article #9004©2000 AAPG/EAGE International Research Conference, El Paso Texas, October 1-5, 2000, 46

MediMap Group., 2005. Morpho-bathymetry of the Mediterranean Sea. CIESM/ Ifremer Special Publication, Atlases and Maps, two maps at 2 000 000.

Meijer, P.T., Krijgsman, W., 2005. A quantitative analysis of the desiccation and re-filling of the Mediterranean during the Messinian Salinity Crisis. Earth and Planetary Science Letters 240, 510-520.

Muñoz, A., Lastras, G., Ballesteros, M.. Canals, M., Acosta, J., Uchupi, E., 2005. Sea floor morphology of the Ebro Shelf in the region of the Columbretres Islands, western Mediterranean. Geomorphology 72, 1-18.

Olaiz, A.J., Muñoz-Martín, A., De Vicente, G., Vegas, R., Cloetingh, S., 2009. European continuous active tectonic strain–stress map. Tectonophysics, 474, 33–40.

Panza, G.F., Raykova, R.B., Carminati, E., Doglioni, C., 2007. Upper mantle flow in the western Mediterranean, Earth and Planetary Science Letters 257, 200-214.

Perea, H., Gràcia, E., Bartolomé, R., Lo Iacono, C., Masana, E., EVENT-SHELF Team., 2009. Structure and potential seismogenic tsunamigenic sources of the

offshore Bajo Segura Fault zone, SE Iberian Peninsula (Mediterranean Sea): preliminary results. Geophysical Research Abstracts 11, EGU2900-B8319, 2009, EGU General Assembly 2009.

Perea, H. Gràcia, E., Bartolomee, R., Lo Iacono, C., Masana, E., 2010. Structure and potential sources of the offshore Bajo Segura Fault Zone, SE Iberian Peninsula (Mediterranean Sea). Looking for the source of the 1828 Torrevieja earthquake. Resúmenes de la 1ª Reunión Sobre Fallas activas y Paleosismologia, Sigüenza, España: 113-116

Pérez Peña, A., Martín-Dávila, J., Gárate, J., Berrocoso, M., y Buforn, E., 2010. Velocity and tectonic strain solutions in southern Spain and the surrounding areas derived from GPS episodic measurements. Journal of Geodynamics, 49: 232–240.

Reches, Z., Baer, G. and Hatzor, Y., 1992. Constraints on the strength of the upper crust from stress inversion of fault slip data. Journal of Geophysical Research 97(B9): doi: 10.1029/92JB02258. issn: 0148-0227.

Reicherter, K.R., Reiss, S., 2001. The Carboneras Fault Zone (southeastern Spain) revisited with Ground Penetrating Radar-Quaternary structural styles from high-resolution images. Netherlands Journal of Geosciences/Geologie en Mijnbouw 80: 129-138.

Riding, R., Braga, J.C., Martín, J.M., Sánchez-Almazo, I.M., 1998. Mediterranean Messinian Salinity Crisis: constraints from a coeval margin basin. Sorbas, southeastern Spain. Marine Geology 46, 1-20.

Robles-Arenas, V., Candela, L., 2010. Hydrological conceptual model characterization band abandoned mine site in semiarid climate. The Sierra de Cartagena-La Unión (SE Spain). Geologica Acta 8, 235-248.

Rouchy, J.M., Caruso, A., 2006. The Messinian Salinity Crisis in the Mediterranean basin: a reassessment of the data and an integrated scenario. Sedimentary Geology 188-189, 35-67.

Rueda, J., Mezcua, J., 2005. Near-real-time seismic moment-tensor determination in Spain. Seismological Research Letters 76 (4), 455-465.

Ryan, W.B.F., 1978. Messinian badlands of the southeastern margin of the Mediterranean Sea. Marine Geology 27, 349-363.

Ryan, W.B.F., Cita, M.B., 1978. The nature and distribution of the Messinian erosional surfaces, indicators of several kilometer-deep Mediterranean in the Miocene. Marine Geology 27, 193-230.

Sábat, F., Roca, E., Muñoz, J.A., Veregés, J., Santanach, P., Sans, M., Mansana, E., Estébez, A., Santisteban, C., 1995. Role of extension and compression in the evolution of the eastern margin of Iberia: the ESCI-Valencia Trough seismic profile. Revista Geológica de España 8, 431-448.

Serpelloni, E., Vannuci, G., Argnani, A., Casula, G., Anzidei, M., Baldi, P., Gsperini, P., 2007. Kinematics of the western Africa-Eurasia plate boundary from focal mechanisms and GSP data. Geophysical Journal International 169, 1180-1200.

Silva, P.G., Goy, J.L., Zazo, C., Bardají, T., 2003. Fault-generated mountain front in southeast Spain: geomorphologic assessment of tectonic and seismic activity. Geomorphology 50, 203-225.

Silva, P,G., Alfaro, P., Masana, E., Martínez Díaz, J.J., Bardají, T., Estévez, A., Goy, J.L., Santanach, P., Zazo, C., Reicherter, K.R., 2004. Active tectonics in the Mediterranean sector of the Iberian Peninsula (east Spain). 32nd International Geological Congress, Florence – Italy, August 20-28, 2004, v.1, B10, 38 pp.

Soria, J.M., Caracuel, J.E., Corbí, H., Dinarés-Turell, J., Lancis, C., Tent-Manclús, J.E., Yébenes, A., 2008. The Bajo Segura Basin (SE Spain): implications for

the Messinian Salinity Crisis in the Mediterranean margins. Stratigraphy 5, 257-263

Stanley, D.J., McCoy, F.W., Diester-Haass, L., 1974. Balearic Abyssal Plain: an example of modern basin plain deformation by salt tectonism. Marine Geology 7, 183-200.

Stich, D., Serpelloni, E., Mancilla, F.L., Morales, J., 2006. Kinematics of the Iberia-Maghreb plate contact from seismic moment tensors and GPS observations. Tectonophysics 426, 295–317.

Vegas, R., 1992. The Valencia Trough and the origin of the western Mediterranean basins. Tectonophysics 203, 249-261.

Vendeville, B.C., 2005. Salt tectonics driven by sediment progradation, part 1: mechanics and kinematics. American Association of Petroleum Geologists Bulletin 89, 1071-1079

Woodside, J.M., Maldonado, A., 1992. Styles of compressional neotectonics in the eastern Alborán Sea. Geo-Marine Letters 12, 111-116.

Woodside, J., Ivanov, M., Koelewjin, R., Zeldenrust, I., Shashkin, P., 2000. South Balearic Basin: the Palomares and Mazarrón margins. Sidescan Sonar Data. Multidisciplinary Study of Geological Processes on the North East Atlantic and Western Mediterranean Margins. IOC Technical Series No. 56, UNESCO, 2000 (English), 95-98.

FIGURE CAPTIONS

Fig. 1. [full page width]

Upper Panel. Bathymetric-tectonic map of SE Spain showing the location of survey area. Thick black line shows the study area (35,269 km^2). Bathymetric contours in meters. Base map from MediMap Group (2005). Additional data from Alfaro et al. (2002a, 2002b), Bousquet (1979), Gràcia et al., (2010), López-Ruiz et al. (2002), Mauffret (2007), Perea et al. (2009), Silva et al. (2003; 2004), Soria et al. (2008) and Robles-Arenas and Candela (2010). **Lower Panel.** DTM of the study area.

Fig. 2 [full page width]

A. DTM of the study area showing the locations of Topas seismic profiles.

B. Map showing the variations in slope angle recorded in the study area based on multibeam bathymetry data.

Fig. 3.

A. 3D bathymetry of the Mar Menor Shelf displaying a chain of northeast trending volcanic ledges off Cabo de Palos. B= Barrier islands; LM=La Manga; PI=Pavement; **B.** 3D of the Mar Menor Shelf imaging 8 relict barriers constructed during the Holocene transgression and recent northeast trending sediment waves between the barriers created by the south flowing North Current. GI= Grosa Islands. **C.** 3D bathymetry of the inner Sierra de Cartagena-La Unión Shelf showing a rocky pavement (PI), with an irregular edge. C=Canyons; F=Fault. **D.** Sediment wave field between Cabo Cope and Águilas. F? =Fault?.

Fig. 4. [full page width]

A: Oblique 3D bathymetry diagram of the Mazarrón and Palomares escarpments. A west-dipping ramp divides the canyons cut into the Mazarrón Escarpment into two groups with that west of the ramp having a more youthful appearance. Note canyon cutting the flank of Seco de Palos Seamount (Psmt). B=Flattop bank with core of Betic Internal Zone rocks; V=Seamount. **B**. 3D bathymetry of the rough terrain at the base of the Mazarrón Escarpment. C=Canyons; F=Fault; OS=Outer Shelf; SE=Shelf's edge; **C:** Close-up of the eastern end of Mazarrón Escarpment. ML=Mar Menor Slope; P=Pockmarks; V= Seamount.

Fig. 5. High-resolution seismic reflection profiles of the Mar Menor (L062) and Sierra de Cartagena-La Unión shelves (011-1111, 010-1111 and 009-1111). B=Barrier Islands; LS?=Lagoonal Sediments deposited behind the barrier islands. R=Ravinement surface eroded during the Holocene transgression on the Betic Internal Zone strata (IZ), T=Terraces; M= Multiple. Along Line 011 the Internal Zone strata are exposed or thinly covered, whereas on lines 010 and 009 IZ is buried. See Fig. 2A for locations of profiles.

Fig. 6. A. High-resolution seismic reflection profile (Line 036-1111) extending from the flat-top high on the southern edge of Mar Menor Shelf to the ramp in the Mazarrón Escarpment. F=Fault; IZ= Bético Internal Zone rocks; R= Ravinement surface eroded during the Holocene transgression; U_1 and U_2= Unconformities. **B.** High-resolution seismic reflection profile (Line 037-1111) extending from the bank in the Mar Menor Shelf to the ramp in the Mazarrón Escarpment. **C**. Seismic reflection profile 035-1111 along the west side of the Mar Menor Slope. 1 and 2=seismic sequences; **D**. High resolution seismic profile 034-1111 along the west side of the Mar Menor Slope, west of the bank on profiles 036-1111 and 037-1111. The sequence along this profile consists of a complex of sediment drift units prograding toward the top of the Mazarrón Escarpment and resting on a strong reflector (IZ) that represents the top of the Bético Internal Zone rocks. See Fig. 2A for locations of profiles.

Fig.7. High-resolution seismic profile (Line 001-1111) demonstrating the seaward facing scarp separating the inner and outer shelves. U=Unconformity; R= Ravinement surface eroded during the Holocene transgression. The south-facing cliff in this and in the profiles in Fig. 5 may represent a sea cliff eroded during the Pleistocene glacially induced regressions. See Fig. 2A for location of profile.

Fig.8. High-resolution seismic reflection profile (Line 063-1111) north of San Pedro Basin. **A.** Torrevieja half-graben. **B.** Elche basin. **C.** Alicante anticlinorium imaging the faulted folds of the structure. Note pockmarks at the top of the faults and the mounds within them that we infer are mud volcanoes. The fault at the NE end of C may be the offshore extension of the Bajo Segura Fault. F=Fault; P = pockmark; M =multiple. See Fig. 2A for locations of profiles.

Fig. 9. High-resolution seismic reflection profiles (055-1111, 051-1111, 049-1111) of the Torrevieja Half-Graben (**A**), and the northwest-southeast trending scarp east of the Mar Menor Slope. The scarp along lines 051 (**B**) and 049 **(C**) is the result of the compression and plastic flow of Messinian evaporites along the fault scarp. F=Faults; MTD = Mass Transport Deposits; AB-B =Algero-Balearic Abyssal Plain. See Fig. 2A for locations of profiles.

Fig. 10. High-resolution seismic reflection profiles (Lines SIS-5-1010 **(A)** and SIS- 8-1010 (**B**) of the Mar Menor Slope (San Pedro Basin). F=Faults; P=Pockmarks; PI= Volcanic Pinnacles; V=Seamount. 3D bathymetry insert shows distribution of circular depressions on the slope that we infer represent pockmarks created by the expulsion of gas/water. See 2A for locations of profiles.

Fig.11. High-resolution seismic reflection profiles of the circular structure in the Algero-Balearic Abyssal Plain. Line 026-1010 **(A)** cuts across the center of the structure and Line 027-1010 **(B)** cuts its southern edge. D=Diapirs with cores of Messinian evaporites. Arabic numbers = relief in meters of diapirs above sea-floor (based on a velocity of 1500 m/sec; same velocity was used in Figs. 12 to 16). F=Faults. FU= Furrow. AB-B= Algero-Balearic Abyssal Plain. See Fig. 2A for locations of profiles.

Fig.12. High-resolution seismic profiles (Lines TD S4-L026 and L009-1111) off the North-South High east of the Mar Menor Slope. We infer that the acoustically transparent mounds are Mass Transport Deposits=MTD; D=Diapirs with cores of Messinian evaporites; F=Faults; PI= Volcanic Pinnacles. See Fig. 2A for location of profiles.

Fig.13. High-resolution seismic reflection profiles (Lines TR L5-L6 and 031-1111) south of the Mazarrón Escarpment. (**A**) The asymmetrical 58 m high on the left is the 50 km long northeast-southwest trending diapiric ridge south of the Mazarrón Escarpment and the structures on the left are the ellipsoid structures north of the ridge. On line 031 (**B**) the ridge is represented by the two diapirs on the right of the profile and the diapirs and warped and faulted sediments on the left side of the profile are

associated with a diapir in the form of a "T". D=Diapirs with cores of Messinian evaporites; F=Faults; SY = Syncline. Arabic numbers are the reliefs in meters of diapirs above sea-floor. See Fig. 2A for location of profiles.

Fig.14. High-resolution seismic reflection profiles of the irregular terrain at the base of the Mazarrón Escarpment west of 0˚30'W. These lines (021-1111 and 022-1111) cut across the terrain in a northwest-southeast and northeast-southwest direction. D=Diapirs; F/TR=Fault or sediment wave Trough. CH = Channel. Arabic numbers are the reliefs of the structures in meters above sea-floor. Features on Line 022 probably represent warped layers bound by faults or sediment waves formed by turbidity currents. We infer that the morphology imaged in these profiles is due to a massive gravitational failure of the Mazarrón Escarpment. See Fig. 2A for locations of profiles**.**

Fig.15. High-resolution seismic profiles of the irregular terrain at the base of the Mazarrón Escarpment at 0˚30'W. Their stratification and proximity of fold structures in Line 026-1111 have led us to speculate that these features may be due either to compression against the Mazarrón Escarpment, rather than the plastic flow of Messinian salt, or gravitational tectonics. The folded massif in Line 024-1111 probably has the same origin. The hummocky surface between two of the structures and the pot holes are the creations of down-slope processes. Arabic number is relief in meters of the higher structures above sea-floor. CH=Channel. See Fig. 2A for locations of profiles.

Fig.16. High resolution seismic profile (007-1111) of the spur trending oblique to the Mazarrón Escarpment, and showing its structural origin. CH=Channel; D=Diapirs; F=Faults. The fault on the west side of the spur is the Tiñoso fault. Arabic umbers indicate relief of diapirs in meters above sea-floor. See Fig. 2A for location of profile.

Fig. 17. [full page width]

Top: Stress inversion results obtained from the focal mechanism nodal planes (Table III) following stress inversion method (Reches et al., 1992). Focal Mechanisms are from Herraiz et al. (2000). Similar results have been calculated for the total population (Left) and for offshore focal mechanisms (Right). Rose diagram shows the active fault orientations deduced for the study area from focal mechanism analysis.

Bottom: Combined topographic and bathymetric map for the study area, with plotted epicenters from Instituto Geográfico Nacional (I.G.N.) and focal mechanism (Table III). Some active faults have been mapped, including kinematics. Black arrows indicate compression and white arrows extension. DTM bathymetric data from this paper. BSF-Bajo Segura-Carrascoy faults; SP=Santa Pola.

Fig. 18. [full page --LANDSCAPE]

Morpho-tectonic-seismic map of the of the region surveyed based on data collected during the present investigation supplemented by data from Alfaro et al. (2002a, 2002b), Camerlenghi et al. (2009), Gràcia et al., (2010), Jiménez-Martínez et al. (2012), López-Ruiz et al. (2002), Maillard and Mauffret (2011), Mauffret (2007), Perea et al. (2009, 2010), Silva et al. (2003; 2004) and Soria et al. (2008).

Table I. Morphometry of the physiographic provinces

Table II. Characteristics of submarine canyons

Table III. Focal mechanisms used to calculate stress tensors following Reches et al. (1992) procedure and plotted in figure17.

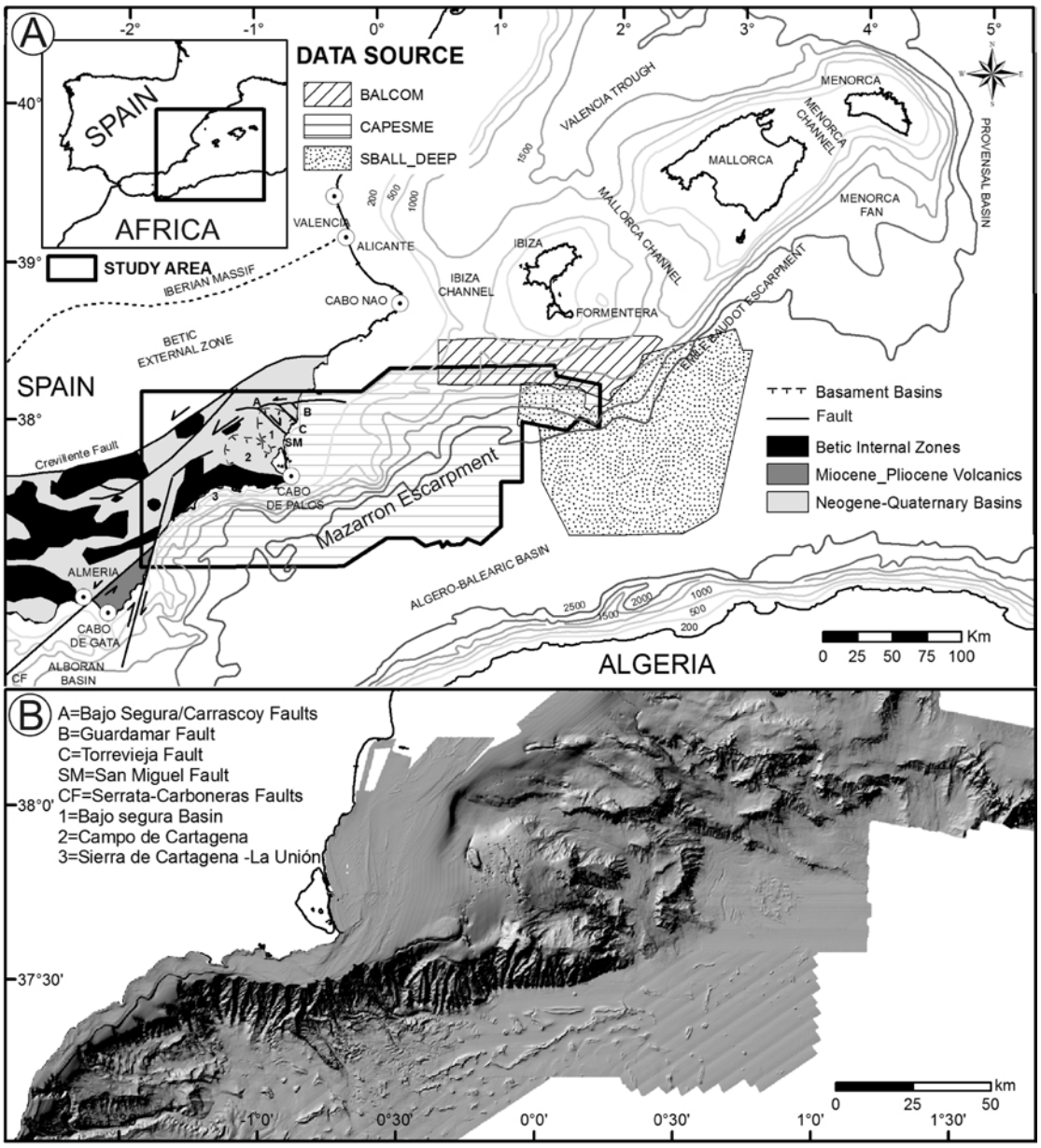
A
DATA SOURCE
BALCOM
CAPESME
SBALL_DEEP
SPAIN
AFRICA
STUDY AREA
IBERIAN MASSIF
BETIC EXTERNAL ZONE
SPAIN
VALENCIA
ALICANTE
CABO NAO
IBIZA
IBIZA CHANNEL
FORMENTERA
VALENCIA TROUGH
MENORCA
MENORCA CHANNEL
MALLORCA
MALLORCA CHANNEL
MENORCA FAN
PROVENSAL BASIN
EMILE BAUDOT ESCARPMENT
Basament Basins
Fault
Betic Internal Zones
Miocene_Pliocene Volcanics
Neogene-Quaternary Basins
Crevillente Fault
CABO DE PALOS
Mazarron Escarpment
ALMERIA
CABO DE GATA
ALBORAN BASIN
CF
ALGERO-BALEARIC BASIN
ALGERIA
Km
0 25 50 75 100
B
A=Bajo Segura/Carrascoy Faults
B=Guardamar Fault
C=Torrevieja Fault
SM=San Miguel Fault
CF=Serrata-Carboneras Faults
1=Bajo segura Basin
2=Campo de Cartagena
3=Sierra de Cartagena -La Unión
km
0 25 50

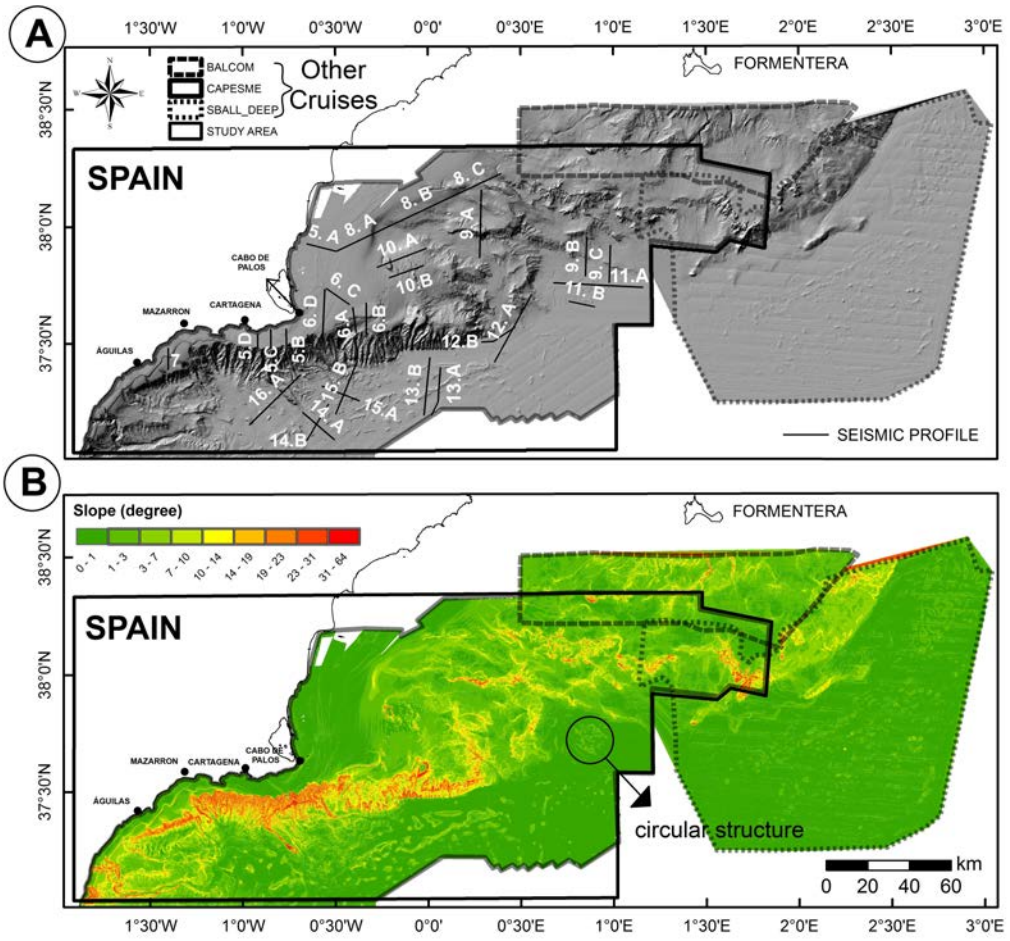
A
1°30'W
1°0'W
0°30'W
0°0'
0°30'E
1°0'E
1°30'E
2°0'E
2°30'E
3°0'E
38°30'N
38°0'N
37°30'N
BALCOM
CAPESME
SBALL_DEEP
Other Cruises
STUDY AREA
FORMENTERA
SPAIN
CABO DE PALOS
MAZARRON
CARTAGENA
ÁGUILAS
SEISMIC PROFILE
B
Slope (degree)
0 - 1
1 - 3
3 - 7
7 - 10
10 - 14
14 - 19
19 - 23
23 - 31
31 - 64
circular structure
km
0 20 40 60

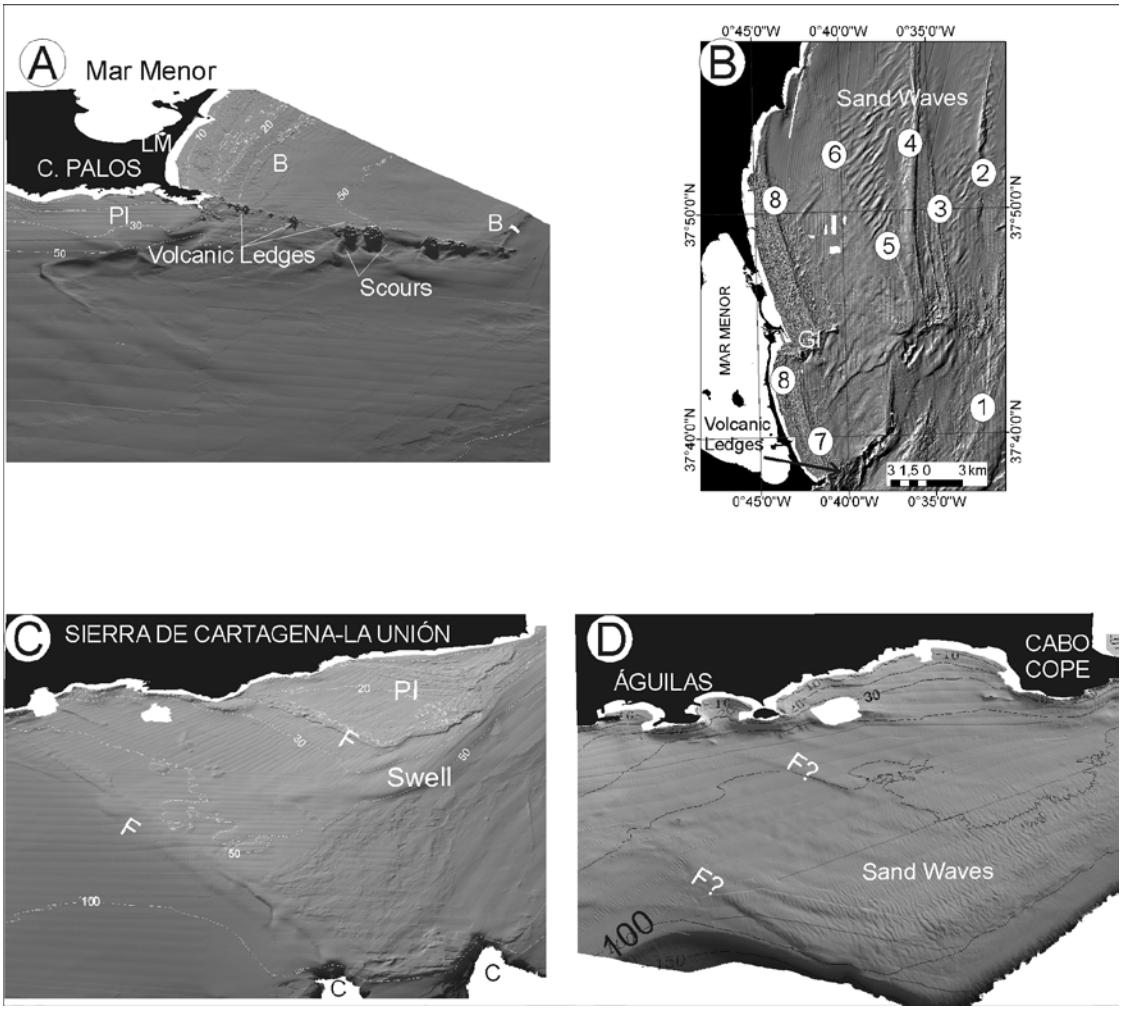
A
Mar Menor
LM
C. PALOS
B
PI30
B
Volcanic Ledges
Scours
B
Sand Waves
0°45'0"W
0°40'0"W
0°35'0"W
37°50'0"N
37°40'0"N
MAR MENOR
Volcanic Ledges
3 1,5 0 3 km
C
SIERRA DE CARTAGENA-LA UNIÓN
PI
F
Swell
F
C
C
D
ÁGUILAS
CABO COPE
F?
F?
Sand Waves
100

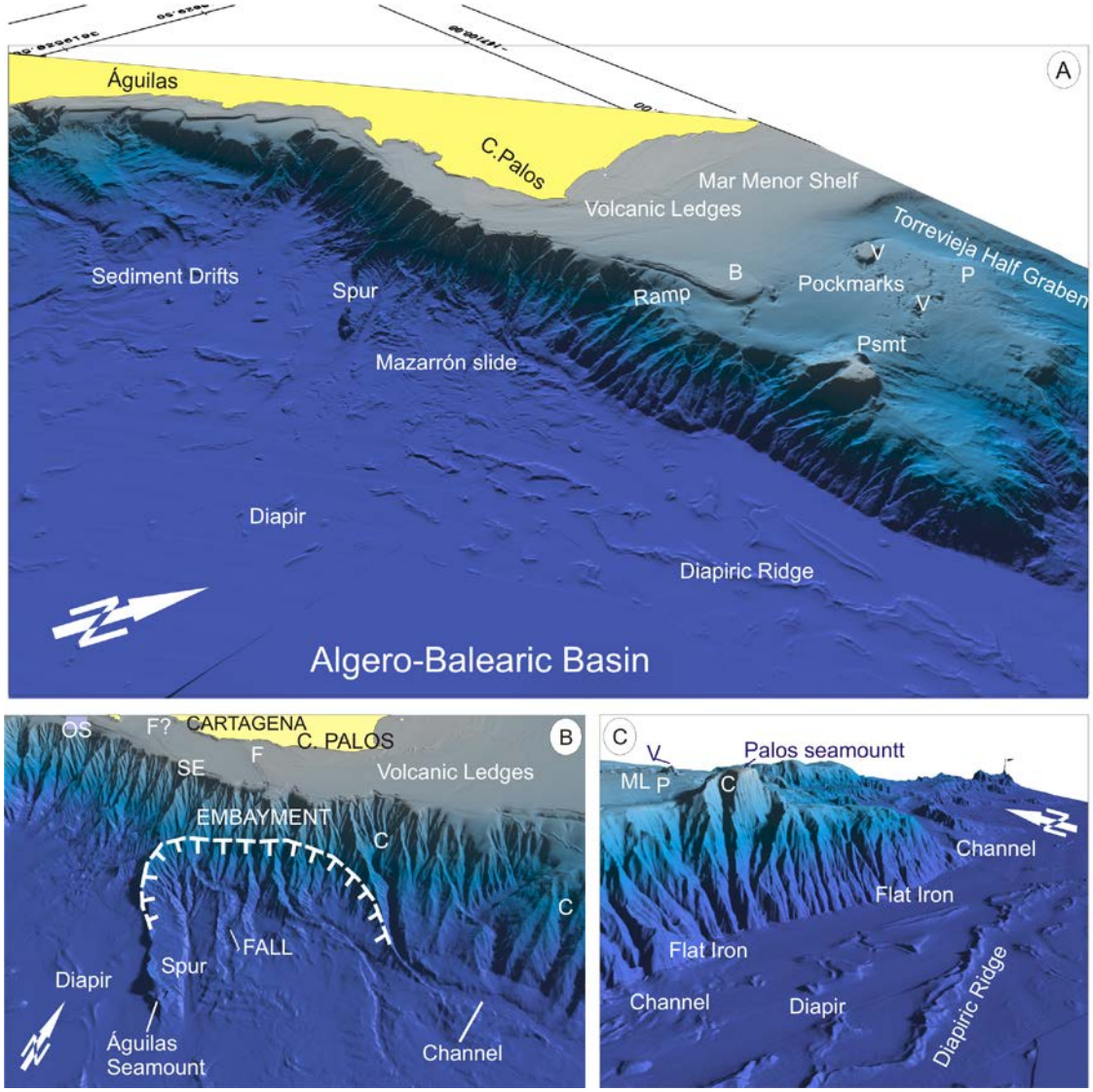
A
Águilas
C.Palos
Mar Menor Shelf
Volcanic Ledges
Torrevieja Half Graben
Sediment Drifts
Spur
Ramp
B
Pockmarks
V
P
V
Psmt
Mazarrón slide
Diapir
Diapiric Ridge
Algero-Balearic Basin
B
OS
F?
CARTAGENA
C. PALOS
F
SE
Volcanic Ledges
EMBAYMENT
C
C
FALL
Spur
Diapir
Águilas
Seamount
Channel
C
V
Palos seamountt
ML P
C
Channel
Flat Iron
Flat Iron
Channel
Diapir
Diapiric Ridge

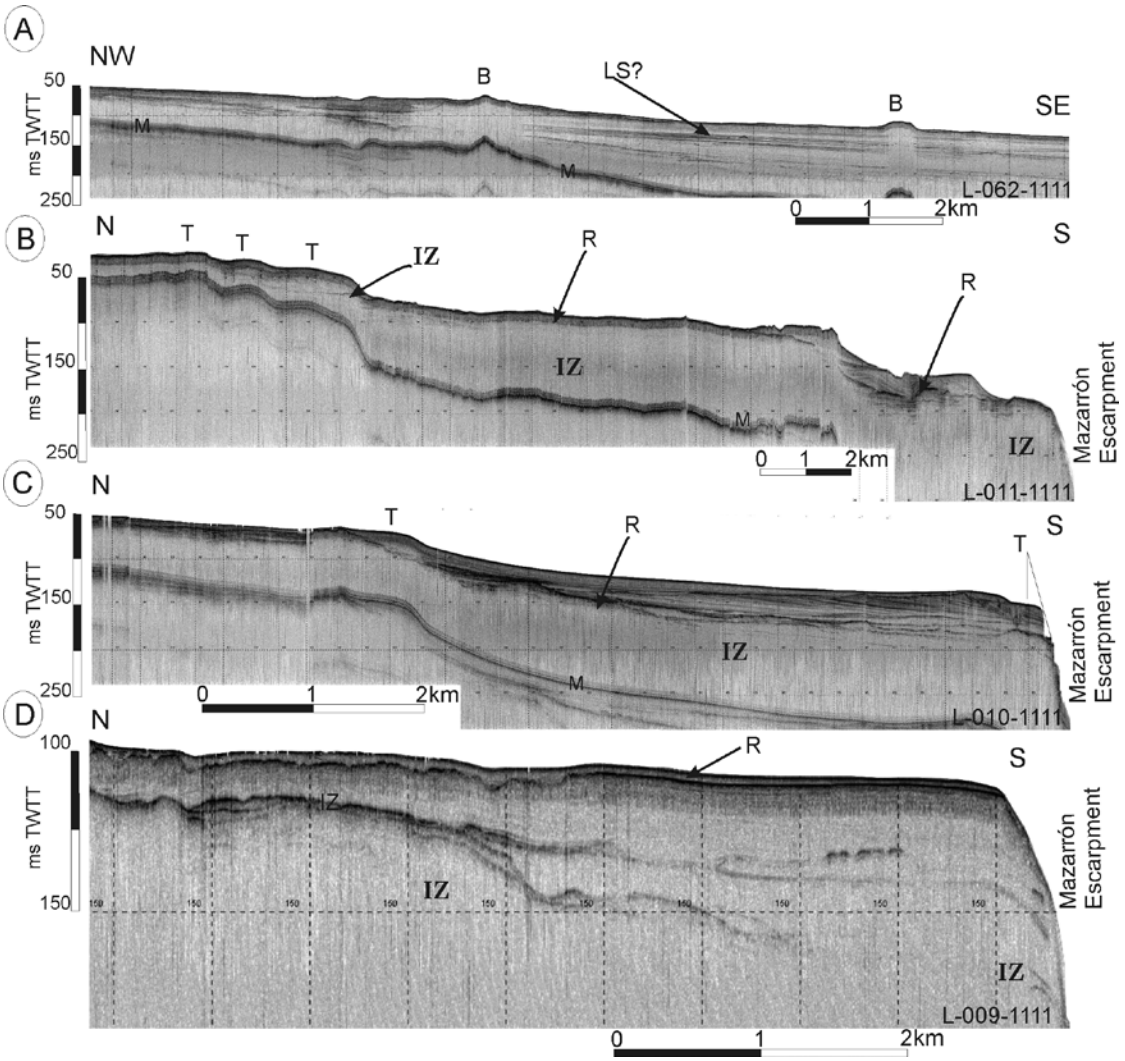
A
NW
SE
B
LS?
B
M
M
50
150
250
ms TWTT
L-062-1111
0 1 2km
B
N
S
T
T
T
IZ
R
R
IZ
M
IZ
Mazarrón
Escarpment
L-011-1111
C
N
S
T
R
T
IZ
M
Mazarrón
Escarpment
L-010-1111
D
N
S
R
IZ
IZ
IZ
100
150
Mazarrón
Escarpment
L-009-1111
0 1 2km

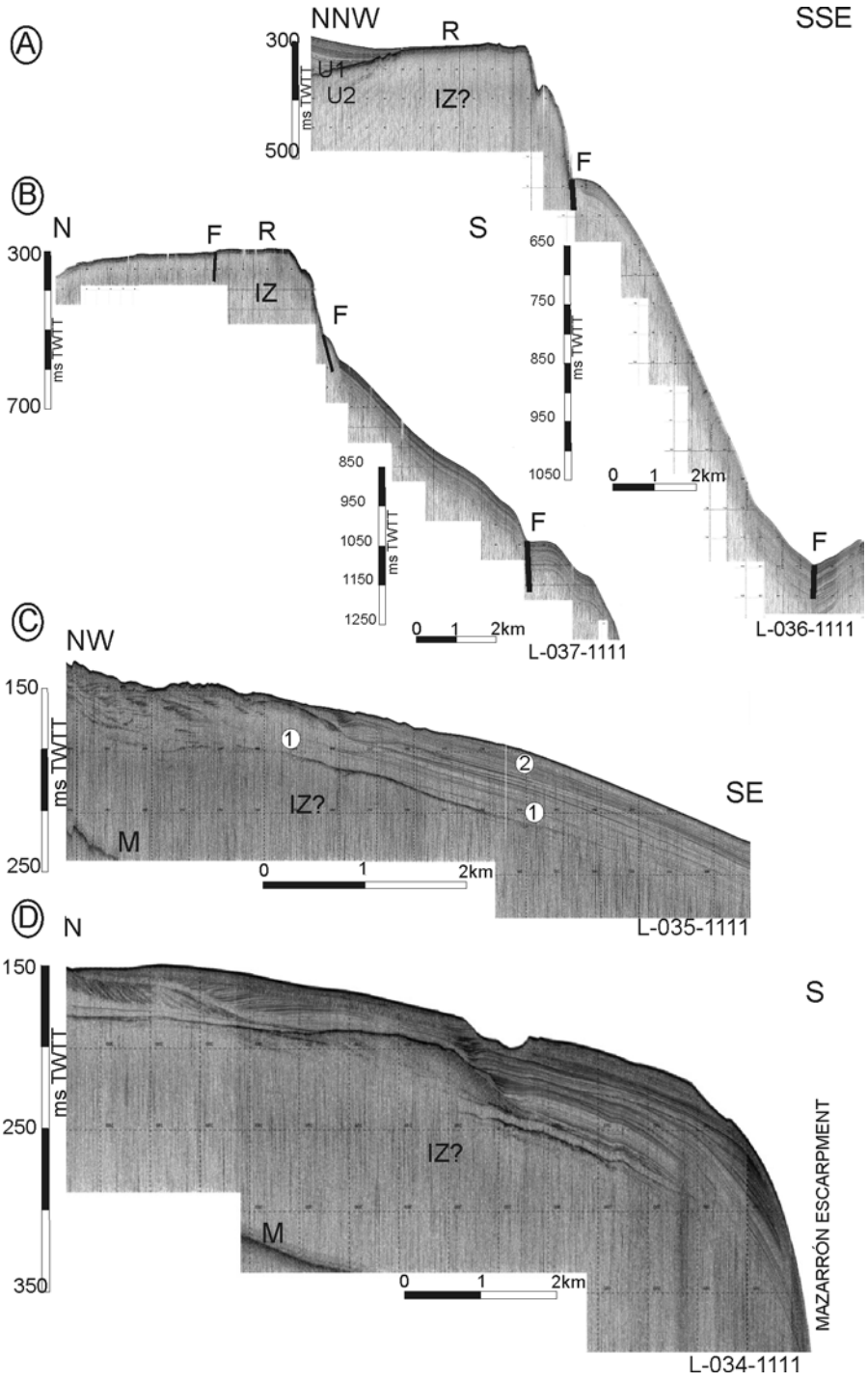
A
NNW
SSE
300
500
ms TWTT
U1
U2
IZ?
R
F
B
N
S
F
R
IZ
F
F
F
300
700
650
750
850
950
1050
850
950
1050
1150
1250
ms TWTT
0 1 2km
L-036-1111
L-037-1111
C
NW
SE
150
250
ms TWTT
1
2
IZ?
M
0 1 2km
L-035-1111
D
N
S
150
250
350
ms TWTT
IZ?
M
0 1 2km
MAZARRÓN ESCARPMENT
L-034-1111

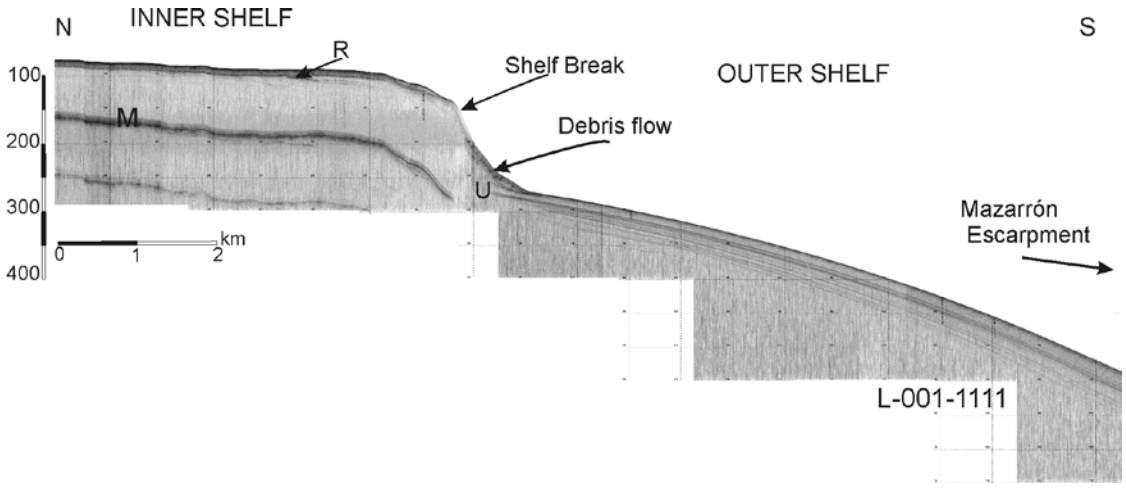
N
INNER SHELF
S
R
Shelf Break
OUTER SHELF
Debris flow
100
200
300
400
M
U
0
1
2
km
Mazarrón
Escarpment
L-001-1111

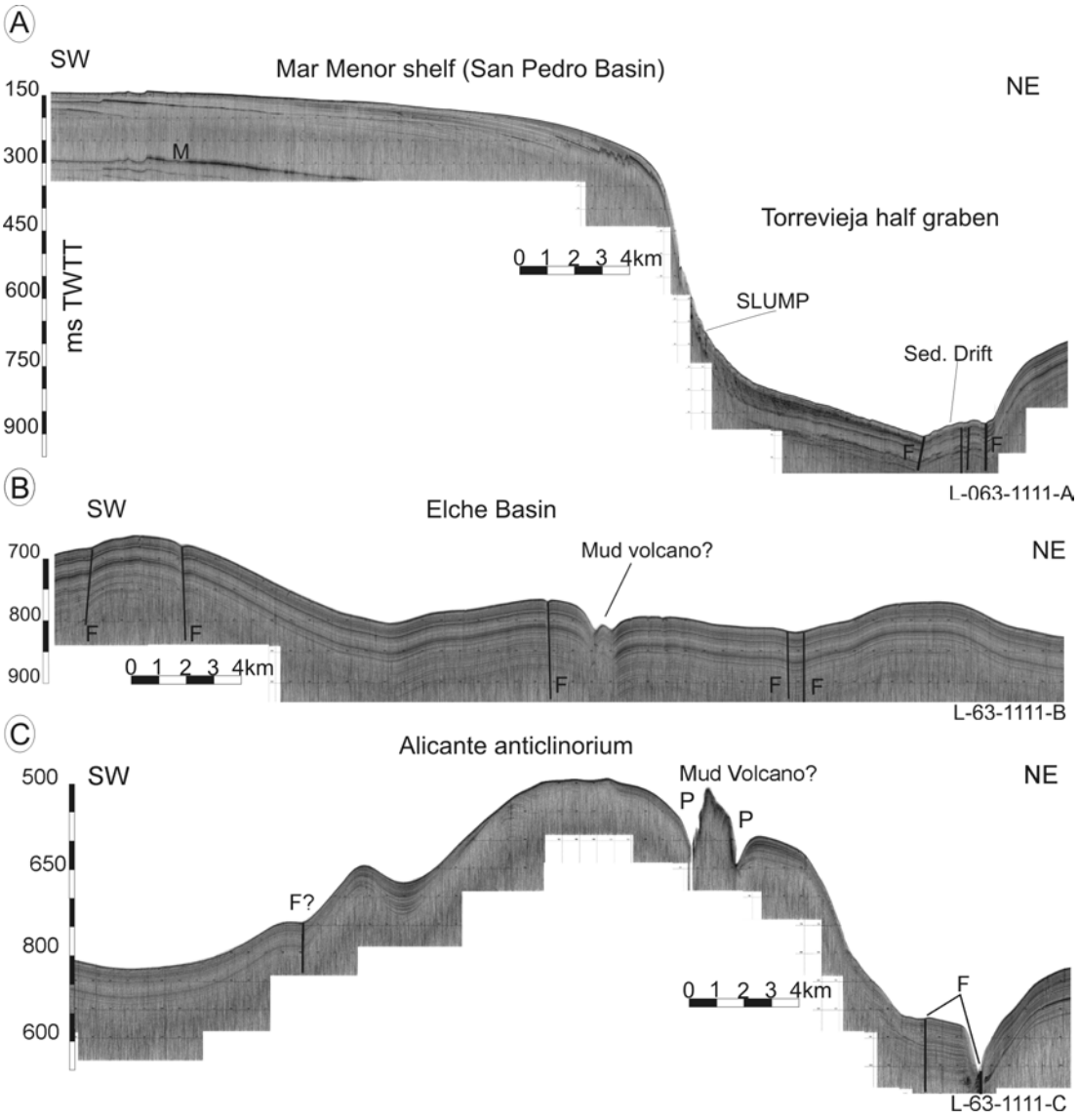
A
SW
Mar Menor shelf (San Pedro Basin)
NE
150
300
450
600
750
900
ms TWTT
M
Torrevieja half graben
0 1 2 3 4km
SLUMP
Sed. Drift
F
F
L-063-1111-A
B
SW
Elche Basin
Mud volcano?
NE
700
800
900
F
F
0 1 2 3 4km
F
F
F
L-63-1111-B
C
Alicante anticlinorium
500
650
800
600
SW
Mud Volcano?
P
P
NE
F?
0 1 2 3 4km
F
L-63-1111-C

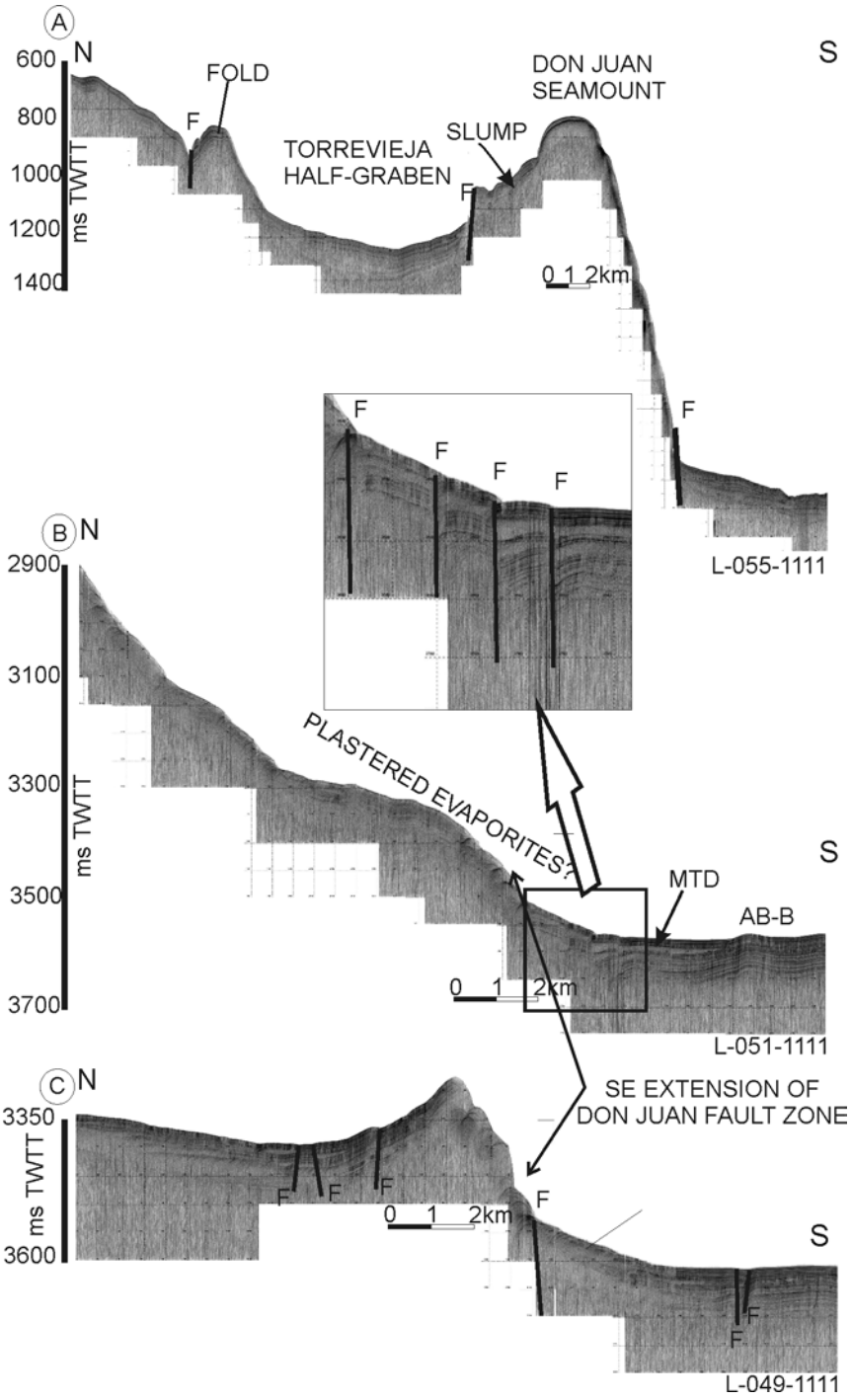
A
N
S
600
800
1000
1200
1400
ms TWTT
FOLD
F
TORREVIEJA
HALF-GRABEN
SLUMP
DON JUAN
SEAMOUNT
0 1 2km
L-055-1111
B
N
S
2900
3100
3300
3500
3700
ms TWTT
PLASTERED EVAPORITES?
MTD
AB-B
0 1 2km
L-051-1111
C
N
S
3350
3600
ms TWTT
SE EXTENSION OF
DON JUAN FAULT ZONE
0 1 2km
L-049-1111

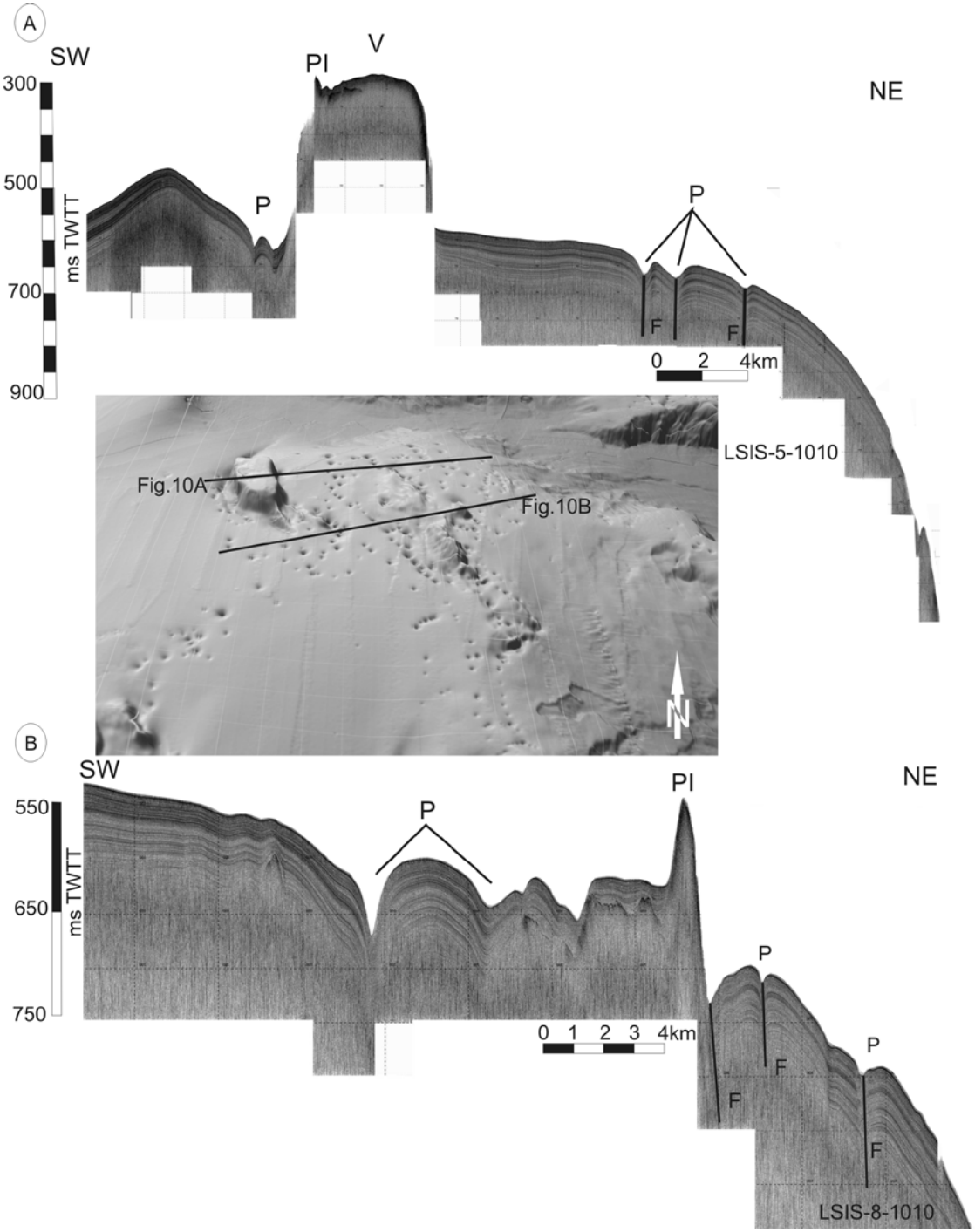
A
SW
NE
PI
V
P
P
300
500
700
900
ms TWTT
F
F
0 2 4km
LSIS-5-1010
Fig.10A
Fig.10B
N
B
SW
NE
PI
P
P
P
F
F
F
550
650
750
ms TWTT
0 1 2 3 4km
LSIS-8-1010

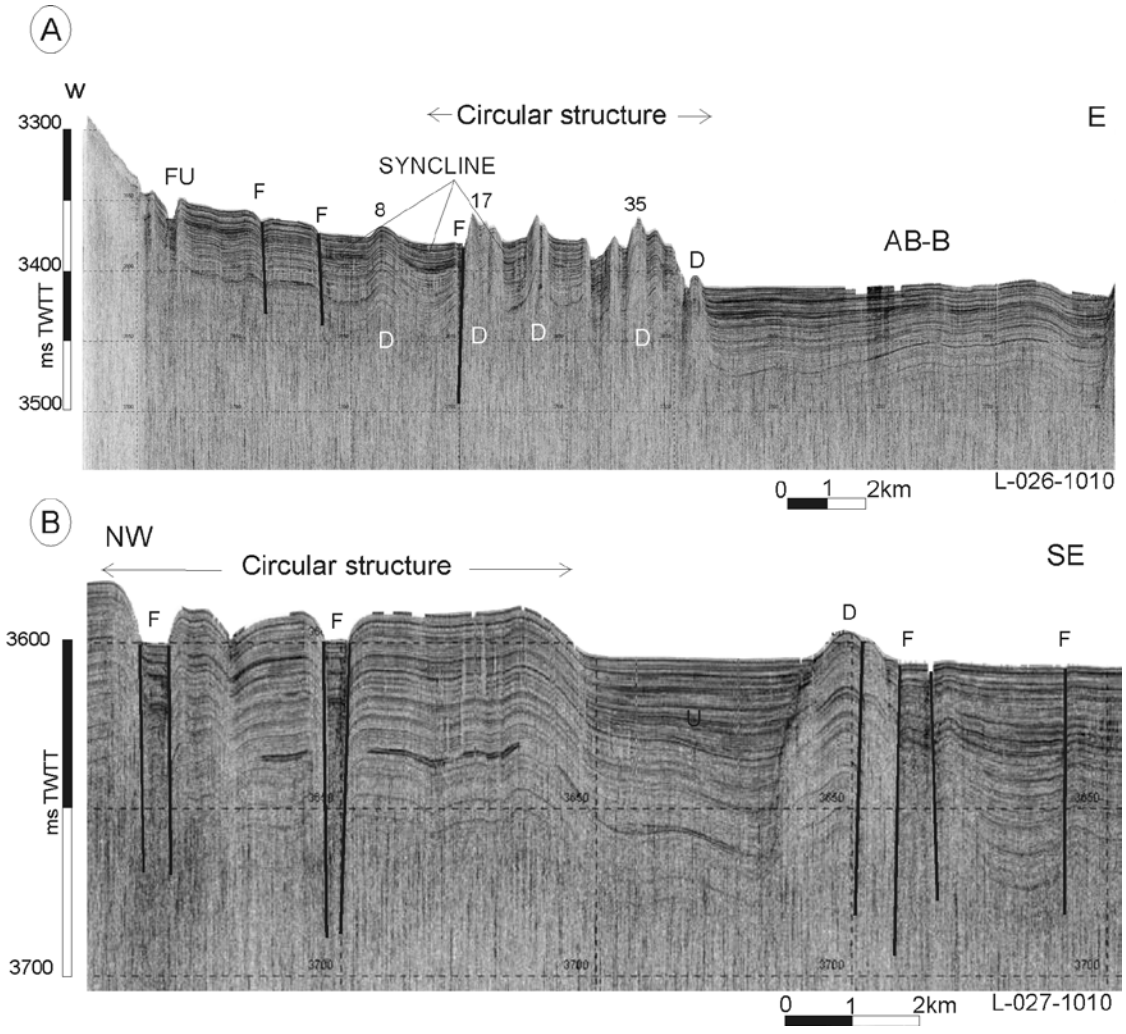
A
W
E
Circular structure
3300
3400
3500
ms TWTT
FU
F
F
8
SYNCLINE
17
F
35
D
AB-B
D
D
D
D
0 1 2km
L-026-1010
B
NW
SE
Circular structure
3600
3700
ms TWTT
F
F
D
F
F
U
0 1 2km
L-027-1010

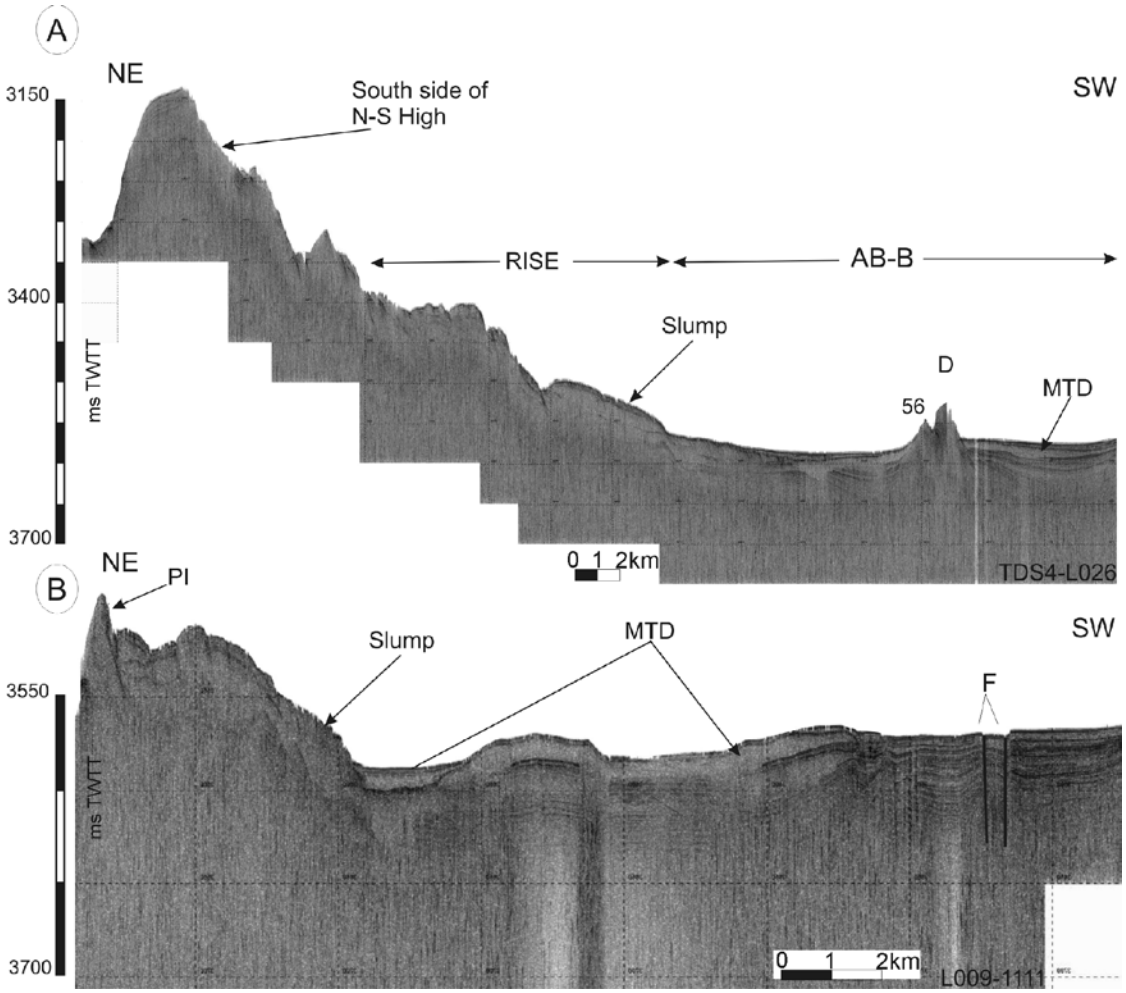
A
NE
SW
South side of
N-S High
3150
3400
3700
ms TWTT
RISE
AB-B
Slump
D
56
MTD
0 1 2km
TDS4-L026
B
NE
PI
SW
Slump
MTD
F
3550
3700
ms TWTT
0 1 2km
L009-1111

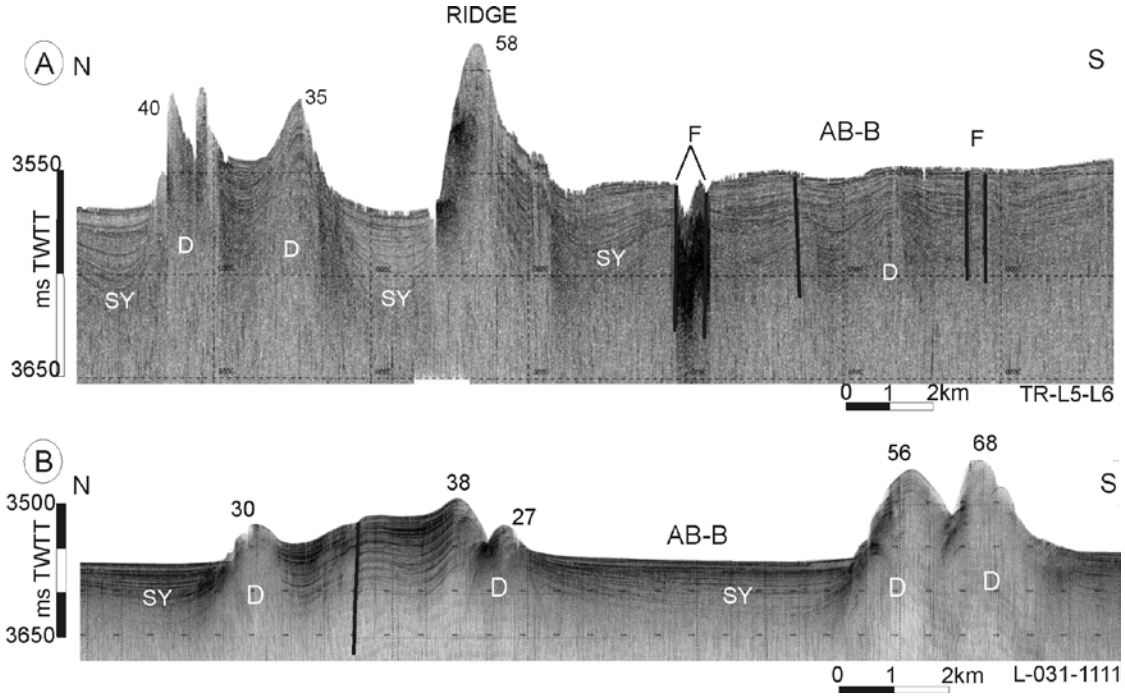
A
N
S
RIDGE
58
40
35
F
AB-B
F
3550
ms TWTT
3650
D
D
SY
SY
SY
D
0 1 2km
TR-L5-L6
B
N
S
56
68
38
30
27
AB-B
3500
ms TWTT
3650
SY
D
D
SY
D
D
0 1 2km
L-031-1111

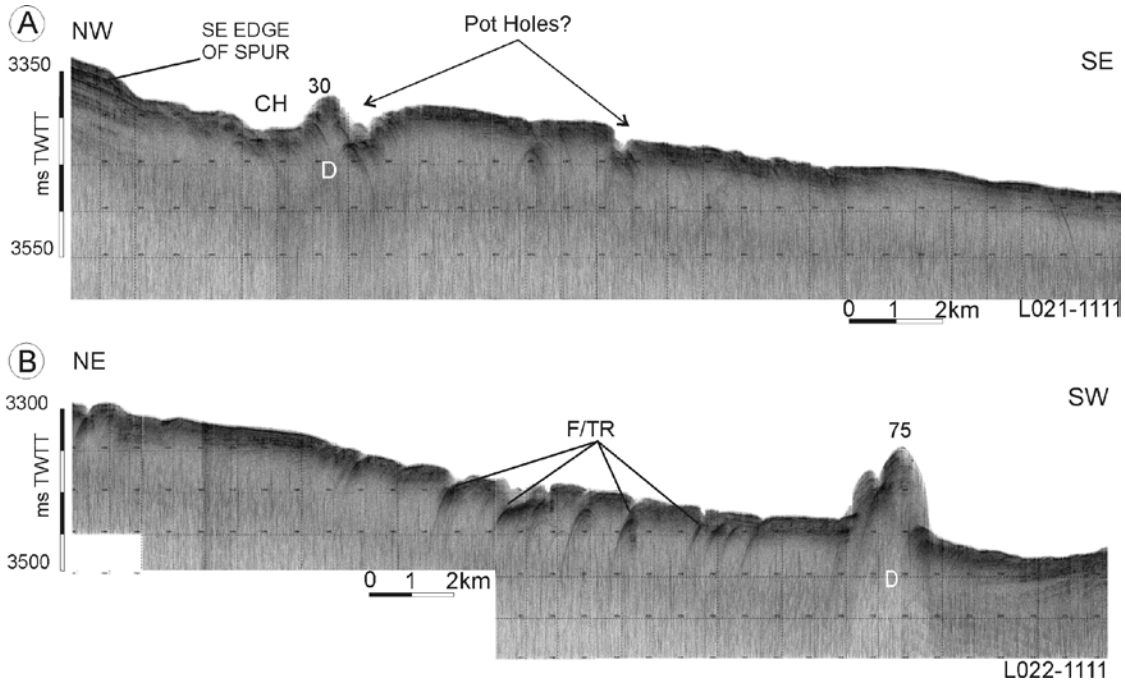
A
NW
SE EDGE
OF SPUR
Pot Holes?
SE
3350
CH
30
ms TWTT
D
3550
0 1 2km
L021-1111
B
NE
SW
3300
F/TR
75
ms TWTT
3500
0 1 2km
D
L022-1111

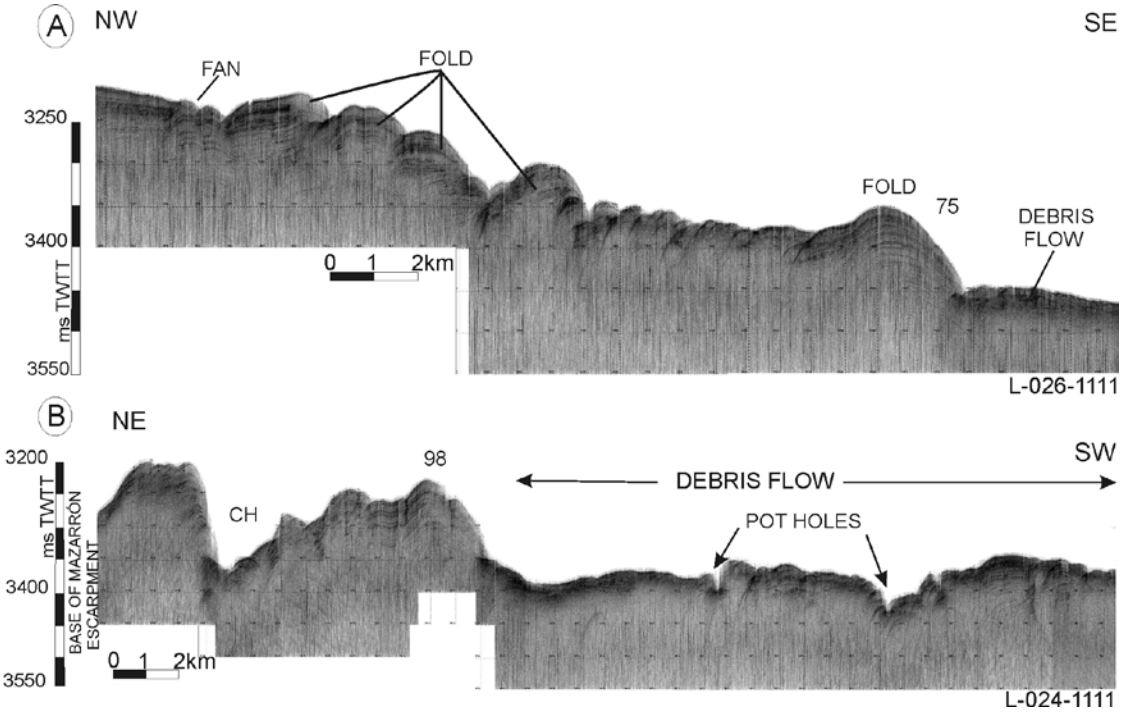
A
NW
SE
FAN
FOLD
FOLD
75
DEBRIS
FLOW
3250
3400
3550
ms TWTT
0 1 2km
L-026-1111
B
NE
SW
98
CH
DEBRIS FLOW
POT HOLES
3200
3400
3550
ms TWTT
BASE OF MAZARRON
ESCARPMENT
0 1 2km
L-024-1111

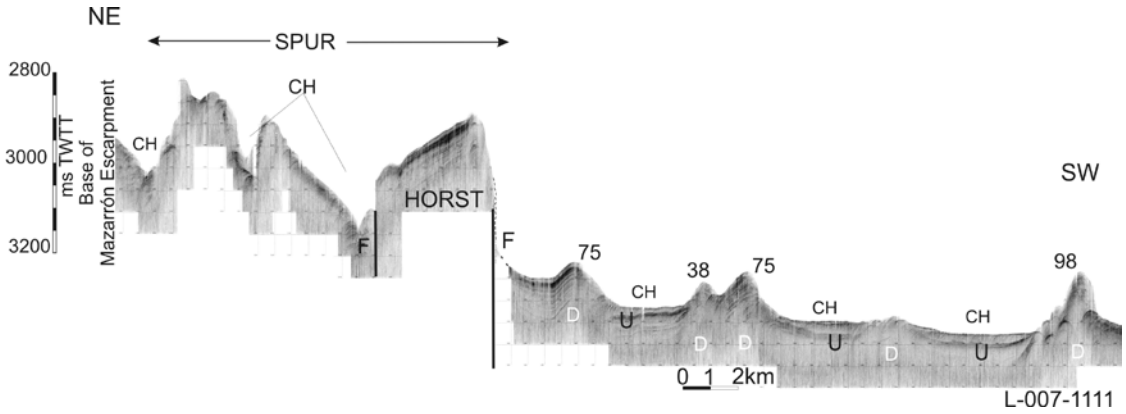
NE
SPUR
2800
3000
3200
ms TWTT
Base of
Mazarrón Escarpment
CH
CH
HORST
F
F
SW
75
38
75
98
CH
CH
CH
CH
D
U
D
D
U
D
U
D
0 1 2km
L-007-1111

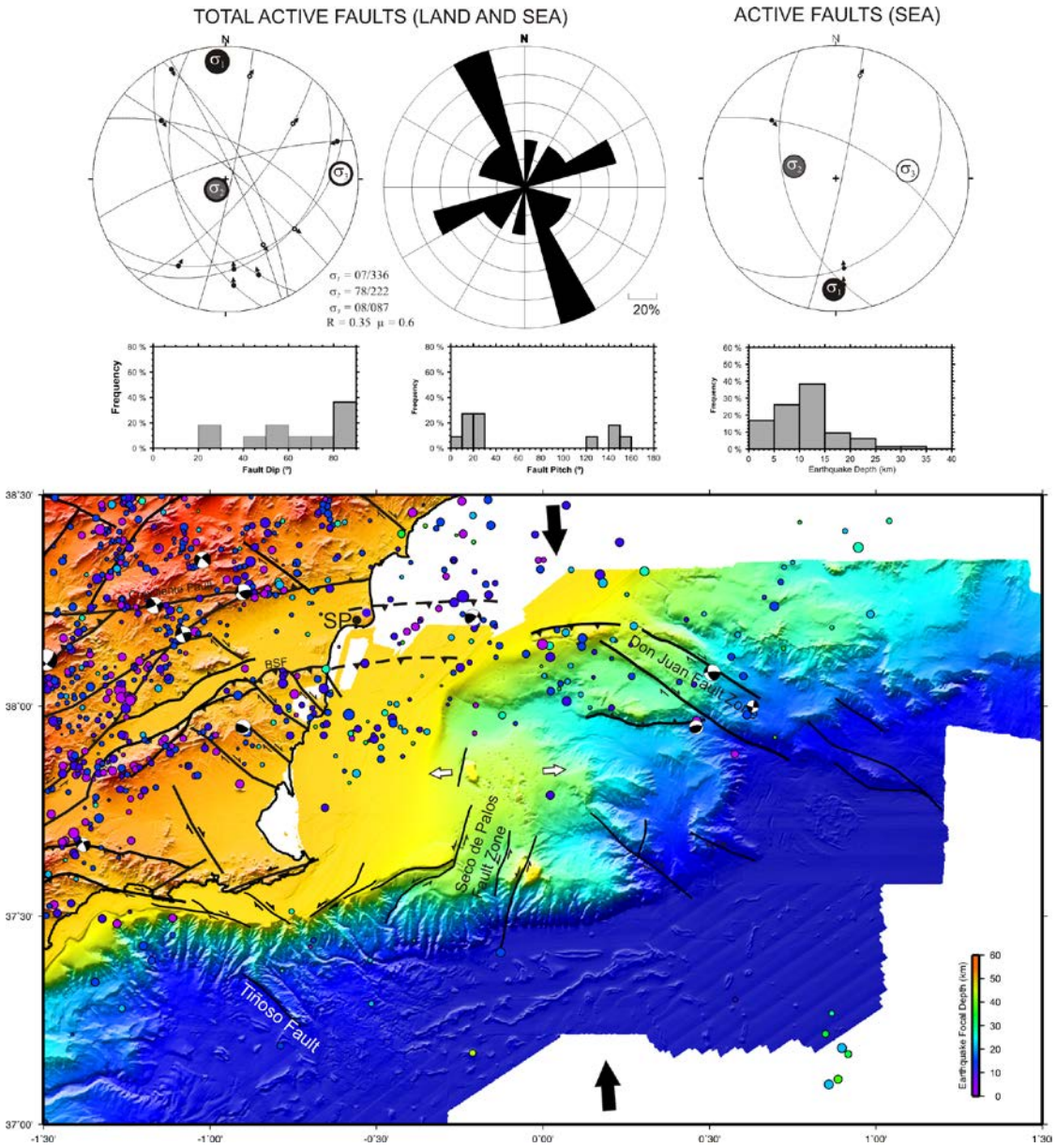
TOTAL ACTIVE FAULTS (LAND AND SEA)
ACTIVE FAULTS (SEA)
N
σ1 = 07/336
σ2 = 78/222
σ3 = 08/087
R = 0.35 μ = 0.6
20%
Frequency
Fault Dip (°)
Fault Pitch (°)
Earthquake Depth (km)
SP
BSF
Don Juan Fault Zone
Seco de Palos Fault Zone
Tiñoso Fault
Earthquake Focal Depth (km)
38°30'
38°00'
37°30'
37°00'
-1°30'
-1°00'
-0°30'
0°00'
0°30'
1°00'
1°30

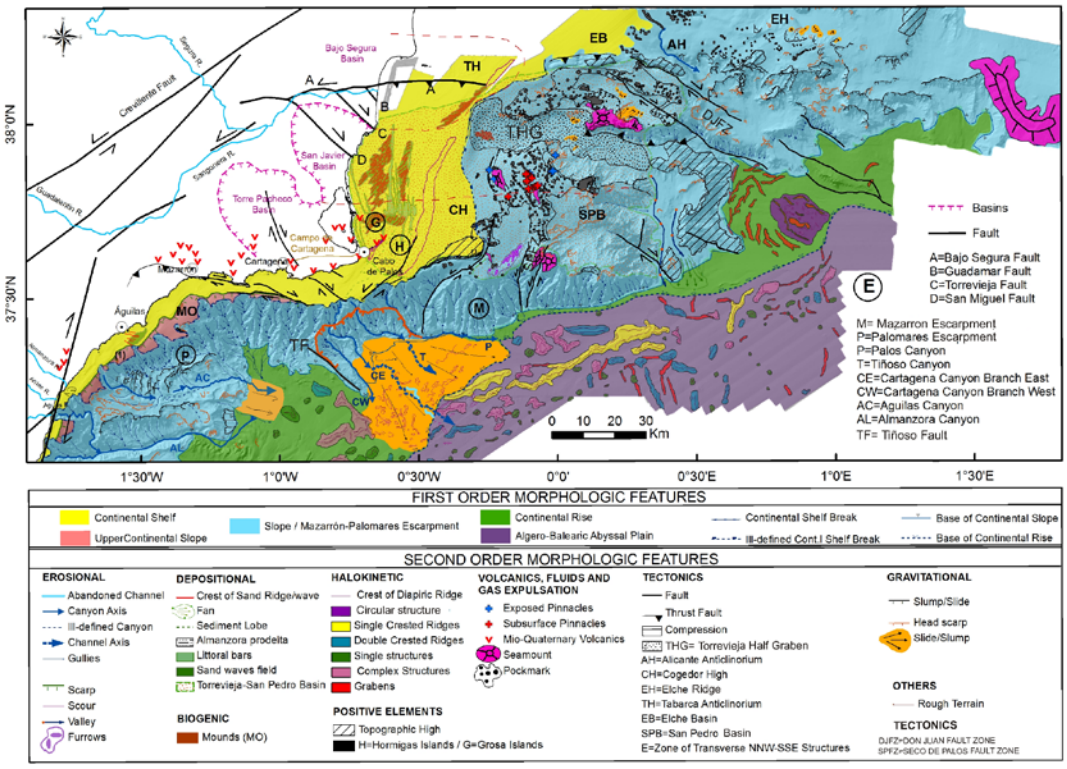
38°0'N
37°30'N
1°30'W
1°0'W
0°30'W
0°0'
0°30'E
1°0'E
1°30'E
0 10 20 30 Km
Bajo Segura Basin
San Javier Basin
Torre Pacheco Basin
Campo de Cartagena
Cabo de Palos
Cartagena
Mazarrón
Águilas
Crevillente Fault
Guadalentín R.
Segura R.
Sangonera R.
Almanzora R.
Aguas R.
EB
AH
EH
TH
THG
CH
SPB
MO
TF
AC
AL
DJFZ
SPFZ
Basins
Fault
A=Bajo Segura Fault
B=Guadamar Fault
C=Torrevieja Fault
D=San Miguel Fault
M= Mazarron Escarpment
P=Palomares Escarpment
P=Palos Canyon
T=Tiñoso Canyon
CE=Cartagena Canyon Branch East
CW=Cartagena Canyon Branch West
AC=Aguilas Canyon
AL=Almanzora Canyon
TF= Tiñoso Fault
FIRST ORDER MORPHOLOGIC FEATURES
Continental Shelf
UpperContinental Slope
Slope / Mazarrón-Palomares Escarpment
Continental Rise
Algero-Balearic Abyssal Plain
Continental Shelf Break
Ill-defined Cont.l Shelf Break
Base of Continental Slope
Base of Continental Rise
SECOND ORDER MORPHOLOGIC FEATURES
EROSIONAL
Abandoned Channel
Canyon Axis
Ill-defined Canyon
Channel Axis
Gullies
Scarp
Scour
Valley
Furrows
DEPOSITIONAL
Crest of Sand Ridge/wave
Fan
Sediment Lobe
Almanzora prodelta
Littoral bars
Sand waves field
Torrevieja-San Pedro Basin
BIOGENIC
Mounds (MO)
HALOKINETIC
Crest of Diapiric Ridge
Circular structure
Single Crested Ridges
Double Crested Ridges
Single structures
Complex Structures
Grabens
POSITIVE ELEMENTS
Topographic High
H=Hormigas Islands / G=Grosa Islands
VOLCANICS, FLUIDS AND GAS EXPULSATION
Exposed Pinnacles
Subsurface Pinnacles
Mio-Quaternary Volcanics
Seamount
Pockmark
TECTONICS
Fault
Thrust Fault
Compression
THG= Torrevieja Half Graben
AH=Alicante Anticlinorium
CH=Cogedor High
EH=Elche Ridge
TH=Tabarca Anticlinorium
EB=Elche Basin
SPB=San Pedro Basin
E=Zone of Transverse NNW-SSE Structures
GRAVITATIONAL
Slump/Slide
Head scarp
Slide/Slump
OTHERS
Rough Terrain
TECTONICS
DJFZ=DON JUAN FAULT ZONE
SPFZ=SECO DE PALOS FAULT ZONE

TABLE I. Morphometry of the physiographic provinces

AREA	*FIRST ORDER MORPHOLOGICAL FEATURE*	*WIDTH max(Km)*	*WIDTH min(Km)*	*WIDTH mean(Km)*	*Depth*	*Shelf Break m*	*Slope Degrees*	*Slope Degrees max*	*Base Slope m*
Mar Menor	Continental Shelf	42	32	37,6	0-200	150-200	0-1	3	_____
Mar Menor	Continental slope	95	50	64	200-2700	_____	3-7	35	2700
Mar Menor	Continental Rise	40	11	19	2450-2770	_____	0-7	_____	_____
Mar Menor	Abyssal Plain	_____	_____	_____	_____	_____	0-1	_____	_____
Mazarrón	Inner Continental Shelf	10,3	2,7	8,2	0-300	100	0-1	_____	_____
Mazarrón	Outer Continental Shelf	4,6	2,5	3	100-300	150-300	0-3	_____	_____
Mazarrón	Continental slope	31,6	17,2	21	300-2700	_____	14-31	64	2700N 2500S
Mazarrón	Continental Rise	24	1,5	_____	2350-2750	_____	1-3	_____	_____
Mazarrón	Abyssal Plain	_____	_____	_____	_____	_____	0-1	12	_____
Águilas/Palomares	Inner Continental Shelf	7,3	0	4,7	0-100	75-100	1-3	_____	_____
Águilas/Palomares	Outer Continental Shelf	8,5	0	3,5- 4	100-450	300-450	1-7	_____	_____
Águilas/Palomares	Continental slope	42	28	38	450-2500	_____	1-7	32	2500
Águilas/Palomares	Continental Rise	61	52	55	2500-2675	_____	0-7	13	_____
Águilas/Palomares	Abyssal Plain	_____	_____	_____	_____	_____	0-1	2	_____

TABLE II. Characteristics of submarine canyons

	Length1 (km)	***Branch length2 (km)***	***Head depth 3 (m)***	***Conf. depth4 (m)***	***Sinuosity5***	***Gradient6***	***knickpoints (m-m´) 7***	***Latitude Longitude (Head)***	***Latitude Longitude (Slope)***	***Latitude Longitude (End)***
Almanzora-Alias-Garrucha	72,437	Branch (N) 30,345	371	1813	1,100	1-7	4(11-34m)	37° 10' 14,978" N 1° 47' 58,145" W	37° 6' 55,023" N 1° 18' 42,01" W	37° 9' 19,159" N 1° 4' 59,023" W
Águilas	54,734	_____	467	_____	1,004	1-10	4(26-93m)	37° 17' 2,606" N 1° 38' 8,644" W	37° 15' 26,013" N 1° 6' 59,042" W	37° 13' 22,641" N 1° 1' 37,563" W
Cartagena (W)	25,726	_____	2058	_____	1,024	1-7	4(3-10 m)	37° 22' 48,795" N 0° 49' 57,687" W	37° 13' 19,213" N 0° 40' 7,36" W	37° 12' 0,362" N 0° 39' 58,787" W
Cartagena(E)	32,292	_____	331	_____	1,374	1-14	5 (36-92 m)	37° 29' 28,294" N 0° 46' 59,275" W	37° 18' 6,997" N 0° 40' 24,505" W	37° 18' 6,997" N 0° 40' 24,505" W
Tiñoso	42,263	_____	471	_____	1,164	1-10	15 (7-40m)	37° 29' 36,91" N 0° 44' 43,213" W	37° 22' 40,79" N 0° 32' 45,862" W	37° 16' 55,08" N 0° 26' 15,8" W
Palos	44,185	_____	1125	_____	1,148	1-14	3(10-43 m)	37° 30' 33,625" N 0° 36' 57,358" W	37° 23' 56,034" N 0° 22' 20,049" W	37° 23' 1,313" N 0° 12' 41,386" W

[1]Total length of the main canyon / branch, including shared path
[2]Length of the branch until it joins the main canyon
[3]Starting depth of the main canyon / branch;
[4]Depth of confluence, at which the branch joins the main canyon
[5]Total sinuosity index over the whole main canyon
[6]Max-Min gradient along the main canyon / branch.
[7]Knickpoints; number and max-min relief of upper/lower sides.

TABLE III. Focal mechanisms used to calculate stress tensors following Reches et al. (1992) procedure and plotted in figure 17.

				nodal plane 1			nodal plane 2				
N	*Longitude*	*Latitude*	*Depth (km)*	*Azimut*	*Dip*	*Rake*	*Azimut*	*Dip*	*Rake*	*Mw*	*Source*
1	-0.2100	38.2100	8	42	66	34	297	59	152	3.7	Stich et al., 2006
2	-1.4900	38.1100	6	41	69	-25	141	66	-157	4.6	Stich et al., 2006
3	0.4600	37.9500	4	49	26	57	265	68	105	3.2	Stich et al., 2006
4	0.6300	38.0000	14	12	85	-13	103	77	-175	2.7	Stich et al., 2006
5	-1.3800	37.6700	4	335	82	-149	240	60	-8	3.2	Stich et al., 2006
6	-1.0800	38.1700	8	253	75	7	162	84	165	3.7	Stich et al., 2006
7	-0.90000	37.9500	4	298	73	113	63	28	38	3.5	Stich et al., 2006
8	-0.90000	38.2700	4	148	51	160	251	74	41	3.7	Stich et al., 2006
9	-1.16740	38.2393	10	64	85	20	332	70	175	3.6	I.G.N.
10	-1.02210	38.3463	3	310	81	-155	216	66	-10	3.8	I.G.N.
11	0.50770	38.0972	3	266	77	44	164	48	163	3.7	I.G.N.